ARTICLE OPEN

Histone deacetylase enzyme activity is not the universal anticancer target of HDAC inhibitors

Chaitra Rai[1], Hang Ruan[2], Xue Li[3], Wenbo Li[1], Hyun-Hwan Jeong[4], Chengchuang Song[1], Panpan Liu[1], Yingjie Chang[3], Hao Fang[3], Udhaya Kumar. S[1], Yuxiang Sun[1], M. James You[5], Dongyin Guan[1], Zhandong Liu[4], Leng Han[6]✉, Xuben Hou[3]✉ and Zheng Sun[1,7]✉

Histone deacetylase inhibitors (HDIs) are approved for treating hematologic cancers and are currently being evaluated in hundreds of clinical trials for various cancers and other diseases, although their mechanisms of action remain poorly understood. Here, our unbiased bioinformatics analyses found that, for most cancer types, expression levels or genetic variants of histone deacetylase (HDACs) do not consistently correlate with carcinogenesis, do not predict cancer patient survival, and do not associate with cellular responses to HDIs. Whole-genome CRISPR library screens did not identify HDACs as genes affecting cellular responses to HDIs. Overexpression of dominant-negative Class I HDACs causes similar protein hyperacetylation as Class I-specific HDI FK228, but does not have similar cytotoxic or transcriptomic effects as FK228 in vitro, and does not alter the anticancer effects of FK228 in vivo in a liver cancer mouse model. Chemical manipulations of a pan-HDI SAHA can abolish its HDAC-inhibiting activity without altering its anticancer effects in vivo in an allograft colon cancer mouse model. These results suggest that HDAC enzyme activity is not necessarily the *de facto* target of HDIs for their anticancer effects. This finding encourages a shift away from a narrow focus on HDACs for understanding HDIs' pharmacodynamics, opening new avenues for developing next-generation compounds for cancers and beyond.

Signal Transduction and Targeted Therapy (2026)11:218 ; https://doi.org/10.1038/s41392-026-02698-1

INTRODUCTION

Histone acetylation is believed to alter chromatin accessibility and regulate gene expression.[1] Histone acetylation at lysine residues is controlled by the catalytic activity of histone acetyltransferases (HATs) and histone deacetylase (HDACs).[2] Mammalian HDACs are grouped into four classes based on sequence homology to their yeast counterparts: Class I Rpd3-like (HDAC1, HDAC2, HDAC3, and HDAC8); Class II Hda1-like (HDAC4, HDAC5, HDAC6, HDAC7, and HDAC9 as class IIa and HDAC10 as class IIb); Class III Sir2-like (SIRT1-7); and Class IV (HDAC11). Class I, II, and IV HDACs share a common zinc-dependent catalytic mechanism,[3] whereas class III HDACs require NAD as the cofactor for their enzymatic activity. The Zn-dependent HDACs show conserved residues at their catalytic sites, including histidine, aspartate, and tyrosine.[3] The tyrosine residue is significant for stabilizing the tetrahedral intermediate at the catalytic site and polarizing the substrate carbonyl for the nucleophilic attack.[3] This key catalytic tyrosine residue is replaced by a histidine residue in class IIa HDACs, rendering them low catalytic activity.[3,4] As a result, Class IIa HDACs enzyme activity is largely dependent on HDAC3, a Class I HDAC.[5]

HDIs inhibit HDAC enzymatic activity by chelating the catalytic zinc ion and blocking its access to substrates.[6] The widely accepted pharmacological model posits that HDIs have three major structural units: a zinc-binding group (ZBG), a cap, and a linker in between.[7] The cap is usually an aromatic, hydrophobic group that interacts with the enzyme's surface. The ZBG can be a hydroxamic acid group or a benzamide group that chelates the zinc ion and directly inhibits the catalytic activity. The potency and selectivity of HDIs vary due to alterations in these groups.[7] HDIs can be classified into different families based on ZBGs. The four most common families of HDIs are aliphatic fatty acids, benzamides, cyclic peptides, and hydroxamic acids.[7] HDIs inhibiting all zinc-dependent HDACs are referred to as pan-HDIs.

Being vigorously pursued by the pharmaceutical industry and actively tested in hundreds of clinical trials,[8,9] HDIs show promise in treating cancers and neurological, inflammatory, and heart diseases. Several HDIs have been approved for cancer. Suberoyl hydroxamic acid (SAHA a.k.a. vorinostat), a hydroxamic acid-based pan-HDI, was approved for cutaneous T-cell lymphoma (CTCL). Belinostat and panobinostat, two hydroxamic acid pan-HDIs, were approved for peripheral T-cell lymphoma (PTCL) and multiple

[1]Department of Medicine, Division of Endocrinology, Diabetes, and Metabolism, Baylor College of Medicine, Houston, TX, USA; [2]Jiangsu Key Laboratory of Infection and Immunity, MOE Key Laboratory of Geriatric Diseases and Immunology, Institutes of Biology and Medical Sciences, Suzhou Medical College, Soochow University, Suzhou, China; [3]Department of Medicinal Chemistry, State Key Laboratory of Discovery and Utilization of Functional Components in Traditional Chinese Medicine, Shandong Key Laboratory of Druggability Optimization and Evaluation for Lead Compounds, School of Pharmaceutical Sciences, Shandong University, Jinan, China; [4]Department of Pediatrics, Duncan Neurological Research Institute, Baylor College of Medicine, Houston, TX, USA; [5]Department of Hematopathology, Division of Pathology and Laboratory Medicine, the University of Texas MD Anderson Cancer Center, Houston, TX, USA; [6]Department of Biostatistics and Health Data Science, School of Medicine, Indiana University, Indianapolis, Indiana, USA and [7]Department of Molecular and Cellular Biology, Baylor College of Medicine, Houston, TX, USA
Correspondence: Leng Han (lenghan@iu.edu) or Xuben Hou (hxb@sdu.edu.cn) or Zheng Sun (zheng.sun@bcm.edu)
These authors contributed equally: Chaitra Rai, Hang Ruan, Xue Li, Wenbo Li

Received: 29 May 2025 Revised: 15 February 2026 Accepted: 17 March 2026
Published online: 05 June 2026

myeloma (MM). However, the FDA withdrew panobinostat in 2021. FK228 (a.k.a. romidepsin), a depsipeptide HDI specific to Class I HDACs, was approved for CTCL and PTCL. Tucidinostat, a benzamide HDI specific to Class I and II HDACs, was approved for PTCL in China and for adult T-cell leukemia-lymphoma (ATLL) in Japan. In our study, we used SAHA, FK228, and MS275[10] as representatives of the hydroxamic acid-based pan-HDI, depsipeptide-based Class I HDAC inhibitor, and benzamide-based Class I HDAC inhibitor, respectively.

Despite their clinical success, HDIs can have toxicity, limited efficacy, and drug resistance.[8,9,11] Defining the molecular basis of their anticancer activity is key to overcoming these challenges and enabling next-generation therapeutics. Since HDACs condense chromatin via histone deacetylation, HDIs are thought to regulate gene expression by increasing histone acetylation. However, HDIs-induced cell death and transcriptional changes do not necessarily correlate with the dissociation kinetic rates of HDIs.[12] The pan-HDI TSA can cause robust histone hyperacetylation with only moderate effects on gene expression.[13] Depletion of HATs in mouse fibroblasts had pronounced effects on histone acetylation but not on gene expression.[14] In addition, different HDIs tend to alter distinct sets of genes in the same cells, with minimal changes in histone acetylation at the promoter regions of these genes.[15] Notably, HDIs do not necessarily affect genes altered by HDAC depletion.[16,17] The most studied HDAC target gene, p21 (CIP1/WAF1), is dispensable for cell cycle arrest upon depletion of HDAC1 and HDAC2.[18] In addition to HDACs, humans have over 300 zinc-dependent enzymes across all six major enzyme families, with conserved tetrahedral coordination in the catalytic site where the zinc ion binds three amino acid residues and a water molecule or hydroxide ion at the fourth position.[19] Thus, HDIs could disrupt other zinc enzymes or metalloproteins beyond HDACs.

In contrast to the seemingly universal anticancer effects of HDIs, HDACs show context-dependent roles in cancer. (1) Loss-of-function mutations in HDACs are positively associated with carcinogenesis, as reported for HDAC1 in liposarcoma patients,[20] for HDAC2 in colorectal/endometrial cancer cell lines and colon tumors,[21,22] and for HDAC4 in melanoma cell lines.[23] There is debate over whether HDAC2 mediates the effects of HDIs.[24,25] (2) Expression levels of HDACs are found to be inversely associated with cancer. Lower expression of HDAC2 and Class II HDACs is associated with poor prognosis and metastasis in colorectal cancer patients[26] and lung cancer patients,[27] respectively. Lower expression of HDAC6 was seen in liver cancer and was associated with increased tumor growth and angiogenesis in xenograft models.[28] Conversely, high expression of HDAC6 was associated with more responsiveness to endocrine treatment and better survival in breast cancer patients.[29] Lack of HDAC1 in a mouse xenograft teratoma model upregulated SNAIL1, a pro-proliferation protein.[30] (3) HDACs are known to be tumor suppressors in some cancers. T-cell-specific deletion of HDAC1 and HDAC2 in the anaplastic large cell lymphoma mouse model increased lymphomagenesis.[31] Knockdown of HDAC1 and HDAC2 accelerates leukemogenesis in a transgenic preleukemic mouse model.[32] Liver-specific depletion of HDAC3 in mice caused hepatocellular carcinoma at around 10–11 months.[33] HDAC2 deletion or knockdown induced epithelial-mesenchymal transition and metastasis.[26] Overexpression of HDAC10 in HeLa cells downregulated MMP2/9 and inhibited cell invasion and metastasis.[34] HDAC11 knockdown increased the metastasis of breast cancer cells from lymph nodes.[35] HDAC6 overexpression in liver cancer cell lines activated caspase-independent autophagic cell death.[36] Thus, HDACs act as tumor suppressors in many contexts. Such context-dependent roles could be due to tissue-specific cofactors or distinct pathway dependencies among different cancer types.

Here, we applied multiple unbiased approaches to investigate the relationship between HDACs and various cancer types. We also performed a genome-wide CRISPR library screen for genes that modulate cellular responses to HDIs. To understand the role of HDAC enzyme activity in the anticancer activity of HDIs, we used catalytically inactive, dominant-negative HDAC tyrosine-to-phenylalanine (YF) mutants and assessed their impact on HDIs activity. Finally, we chemically modified pan-HDI SAHA to test whether its HDAC-inhibitory activity can be dissociated from its anticancer effects. To avoid bias toward a single cancer type, we examined multiple solid tumor models in which HDIs are actively being tested clinically. Our study suggests that HDAC-inhibitory activity is not required for the anticancer effects of HDIs.

RESULTS

HDAC genetic variants or expression do not correlate with most cancers or cancer patient survival

HDAC1, 3, and 11 were aberrantly expressed in multiple cancer types and associated with prognosis in different cancers.[37–39] In contrast to context-specific correlations of HDACs, HDIs have consistently demonstrated anticancer effects, either as monotherapy or in combination therapies, although their efficacy has not yet warranted approval for certain cancer types, which might be attributed to the pharmacological profiles of currently available compounds. We conducted a series of unbiased bioinformatics analyses of HDAC by leveraging public databases. None of the HDACs show consistent differential gene expression patterns between tumor and non-tumor tissues across major cancer types in The Cancer Genome Atlas (TCGA) database (Fig. 1a and Supplementary Table S1). Cancer types with over five paired tumor-normal samples are selected for the differentially expressed gene (DEG) analysis (Supplementary Table S2). Some HDACs, such as HDAC4, are downregulated in breast cancer (BRCA) and thyroid cancer (THCA) compared to normal tissues, which contradicts their presumed oncogenic role. By comparison, the expression levels of canonical oncogenes and tumor suppressor genes show consistent positive and negative correlations with major cancer types, respectively (Fig. 1b). Next, we analyzed the relationship between the HDAC gene expression levels and cancer patient survival using the TCGA database. There is no consistent correlation between HDAC gene expression levels and hazard in most cancers (Fig. 1c). For example, high HDAC11 expression was associated with a low survival rate in acute myeloid leukemia (LAML) but a high survival rate in diffuse large B cell lymphoma (DLBC) (Fig. 1d), suggesting that HDAC11 might play opposite roles in different cancer types. Our result with AML aligns with previous reports that high HDAC11 level is associated with poor overall survival in patients with AML.[38,40] By comparison, expression levels of canonical oncogenes or tumor suppressors consistently show negative or positive correlations, respectively, with patient survival (Supplementary Fig. S1 and Table S3). We then examined the genetic variants in HDACs. HDACs show a low mutation rate in cancers (Fig. 1e). By comparison, canonical oncogenes or suppressor genes TP53, PTEN, or EGFR have a much higher mutation prevalence in cancers (Fig. 1e).

Our results are consistent with the largely negative findings from several recent analyses. Pan-cancer whole-genome sequencing studies did not identify HDACs as recurrently mutated oncogenes or tumor suppressors,[41] suggesting that HDAC function in cancer is more likely to be activity-based than mutation-driven. HDACs are also not enriched among biomarkers of response or resistance to immunotherapy in clear cell renal cell carcinoma.[42] In a multi-omic machine-learning study predicting therapy response,[43] HDAC genes were included in expression matrices but did not emerge as top predictive features. Similarly, analysis of over 10,000 cancer genomes failed to identify HDAC genes as cancer drivers, despite strong signals from other chromatin regulators such as ARID1A, SMARCA4, and KMT2D.[44] Large real-world clinicogenomic datasets further indicate that HDAC alterations are rare and not predictive when compared with

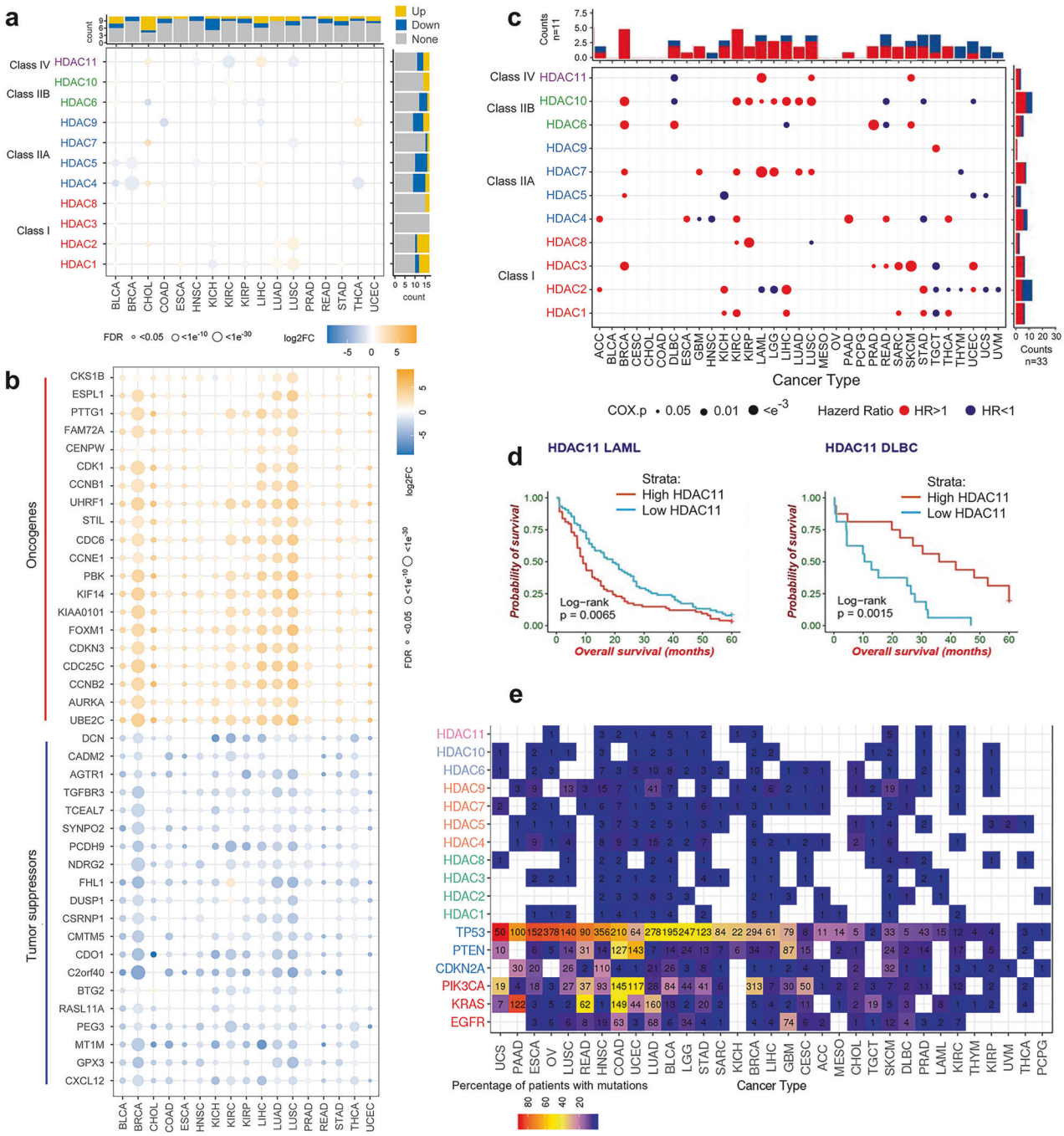

Fig. 1 Gene expression levels and genetic variations of HDACs do not have a consistent correlation with cancer. **a** Gene expression profiles of HDACs across different cancer types from the Cancer Genome Atlas Program (TCGA) database. For the abbreviations for different cancers in the TCGA database, please refer to https://gdc.cancer.gov/resources-tcga-users/tcga-code-tables/tcga-study-abbreviations. The count on the x-axis indicates the number of HDACs, while the count on the y-axis indicates the number of cancer types. **b** Gene expression profiles of classical oncogenes or tumor suppressors in different cancers from the TCGA database. **c** Hazard ratios (HR) of high HDAC gene expression on patient survival from the TCGA database. **d** Correlation between the HDAC11 expression level and the survival of patients with acute myeloid leukemia (LAML) or diffuse large B-cell lymphoma (DLBC). High or low HDAC11 groups consist of samples with HDAC11 expression levels above or below the median levels in the TCGA cohorts (Top or bottom 50%). **e** Prevalence of genetic variants in HDACs and classical oncogenes or tumor suppressor genes in different cancer types from the TCGA database. The number in the heatmap shows the number of patients with mutations

canonical oncogenes (e.g., EGFR, KRAS, TP53) or DNA-repair genes.[45] Single-cell RNA-seq analyses of multiple solid tumors did not reveal HDAC-specific dependencies predictive of drug response.[46] HDACs were neither biomarkers nor mechanistic mediators in a study focused on biallelic tumor suppressor inactivation.[47] A pan-cancer transcriptional analysis of histone acetylation enzymes identified five molecular groups and suggested that Group II may benefit from pan-HDAC inhibitor treatment compared to Group V. However, comparison of Group II with Group V revealed lower expression of HDAC4, 5, 6, 9, and 11, higher expression of HDAC1 and HDAC7, and no obvious changes in HDAC2 or HDAC10.[48]

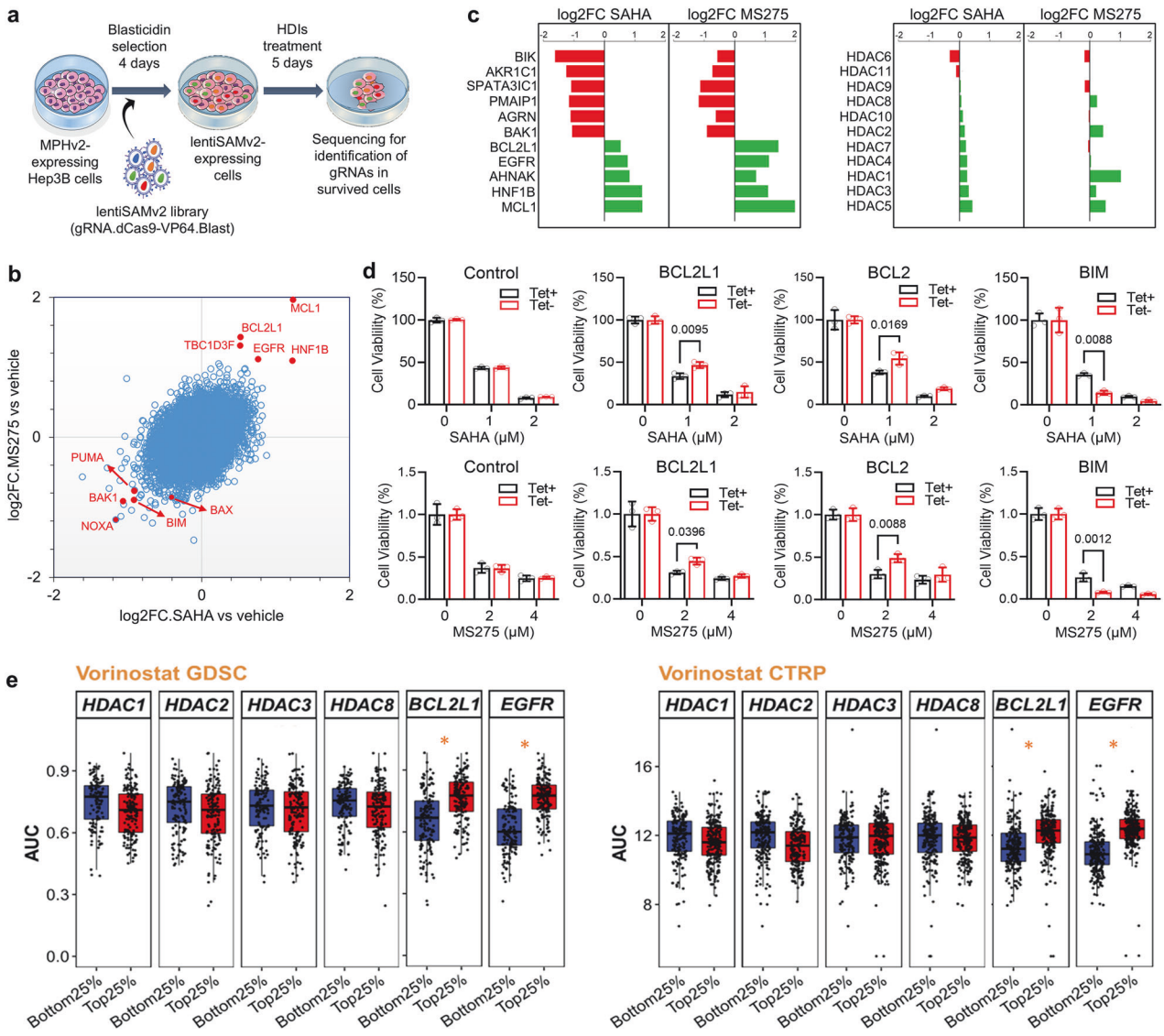

Fig. 2 CRISPRa library screen did not identify HDACs as modulators of cellular response to HDIs. **a** Graphical representation of the CRISPRa library screen. **b** Scatter plot of genes that are positively or negatively enriched after treatment with SAHA or MS275. Fold-change (FC) was presented on the $\log_2$ scale. **c** Fold-change (FC) of top enriched genes and HDAC genes after SAHA or MS275 treatment compared to the vehicle control. **d** Relative cell viability in response to the indicated HDI treatment in Hep3B stable cell lines overexpressing the indicated BCL2 family member using the inducible Tet-OFF system ($n = 3$ experiments). Transgene expression was induced after withdrawal of doxycycline (Tet-). Data are presented as the mean ± SD. Significance was tested by 2-way ANOVA and Bonferroni's tests. *p*-values are as indicated. **e** Correlation of gene expression levels of HDACs or enriched genes (top vs. bottom 25%) with the cellular sensitivity to vorinostat (SAHA) in the Genomics of Drug Sensitivity in Cancer (GDSC) and the Cancer Therapeutics Response Portal (CTRP) database. A higher area under the curve (AUC) value from the dose-response curve of vorinostat indicates more resistance to drug-induced cytotoxicity. Significance was tested by the Mann-Whitney U test. * indicates significance

These unbiased analyses suggest that HDACs are unlikely to be universal oncogenes or tumor suppressor genes, which contrasts with the consistent anticancer effects of HDIs across different cancer types. These results do not exclude the possibility that HDACs can function as oncogenes in specific contexts. Such context-dependent roles could be due to tissue-specific cofactors or distinct pathway dependencies among different cancer types.

CRISPR library screen did not identify HDACs as genes affecting cellular responses to HDIs

To further explore the mechanism underlying the anticancer effects of HDIs, we took another unbiased approach, genome-wide CRISPR library screening. Overexpression or amplification of drug-targeted genes can often confer drug resistance.[49] Several HDACs are considered essential genes for cell survival and would be undetectable in drug response screens using a loss-of-function approach. Therefore, we used a gain-of-function CRISPR activation (CRISPRa) library to identify genes that can modulate HDI-mediated cytotoxicity. The CRISPR/Cas9-based Synergistic Activation Mediator version 2 (SAMv2) system targets gene promoters and enables site-specific transcriptional activation of the gene of interest.[50] We used the human CRISPRa library targeting 23,430 genes or gene isoforms, with three guides per gene, for a total of 70,290 guides. We delivered the lentivirus library into Hep3B cells, selecting cells infected with vectors for MS2-p65-HSF1 (MPH) and gRNA/dCas9-VP64 using hygromycin and blasticidin, respectively. Cells were then treated with vehicle or HDIs (SAHA or MS275) for 5 days before collection for DNA extraction and sequencing (Fig. 2a). We

used SAHA and MS275 as representatives of hydroxamic acid-based and benzamide-based HDIs, respectively, to identify modulators shared across distinct HDIs groups. We used the whole-genome library for this screen because we wish to provide novel insights into the genuine HDIs targets. The concentration of HDIs was optimized so that 10% of cells were viable after 5 days (Supplementary Fig. S2). We chose this long-exposure, low-dose regimen over a short-duration, high-dosage regimen because we think that the former mimicked the in vivo situation better and allowed a longer time window for compensatory mechanisms to kick in. We reason that high-dose HDIs might have more nonspecific effects and kill cells too quickly, leaving no room for compensation. The sequencing data were analyzed using the CRISPRBetaBinomial (CB^2) algorithm to assess enrichment at both guide and gene/isoform level.[51] The complete list of enriched genes was provided (Supplementary Table S4). Gene enrichment shows a moderate but positive correlation between SAHA and MS275 compared to the vehicle control ($r = 0.3744$) (Fig. 2b), suggesting the existence of overlapping and non-overlapping mechanisms underlying cellular responses to these two different HDIs. Importantly, HDAC genes were not consistently enriched. Instead, genes involved in apoptosis and proliferation showed robust enrichment (Fig. 2c). Specifically, the anti-apoptotic/pro-proliferation genes *BCL2L1*, *MCL1*, and *EGFR* were positively enriched in the HDIs-treated group compared to the vehicle control. In contrast, the pro-apoptotic/anti-proliferation genes, such as BIK, PMAIP1, and BAK1, were negatively enriched in the same comparison (Fig. 2c). Only 5 and 6 out of the top 200 enriched genes after SAHA and MS275 treatment have direct physical interaction with HDACs or HDAC-interacting proteins (Supplementary Fig. S3), using the list of HDAC-interacting proteins obtained from BIOGRID[4.4] (Biological General Repository for Interaction Datasets) (Supplementary Table S5).

We sought to independently validate the screening results by constructing Hep3B stable cell lines overexpressing several BCL2 family members. To avoid the effect of transgene overexpression on baseline cell viability or proliferation, we used recombinant lentivirus with the tetracycline-controlled Tet-OFF system to allow transgene overexpression only after HDIs were added. The stable cell lines were maintained in medium supplemented with a tetracycline analog (Tet +) to suppress transgene expression. We withdrew tetracycline analog (Tet-) and added HDIs simultaneously. Such inducible expression of anti-apoptotic BCL2L1 or BCL2 counteracted the cytotoxicity of SAHA or MS275, as measured by the Cell Counting Kit-8 (CCK-8) (Fig. 2d and Supplementary Fig. S4). Similarly, inducible overexpression of pro-apoptotic BIM potentiated HDI-induced cytotoxicity (Fig. 2d and Supplementary Fig. S4). To explore whether the conclusion applies to other cancer cell lines, we examined the relationship between cellular responses to HDIs and the gene expression levels of BCL2L1, EGFR, and HDACs using data from the GDSC (Genomics of Drug Sensitivity in Cancer) and CTRP (Cancer Therapeutics Response Portal) databases. The cell lines were stratified into two groups based on RNA levels of HDACs, BCL2L1, or EGFR (top 25% vs. bottom 25%). The groups with high BCL2L1 or EGFR expression, but not HDAC expression, showed a bigger area under the curve (AUC) in the cell viability dose-response curves plot after vorinostat (SAHA) treatment, suggesting resistance to SAHA-induced cell death (Fig. 2e). Thus, the pharmaceutical profiling data in GDSC and CTRP support our CRISPR library screen results and suggest that HDI-induced cellular responses are modulated by the BCL2 gene family but not necessarily by HDACs.

The finding that the BCL2 family modulates HDIs response is in line with prior studies. Overexpression of BCL2 in HeLa cells, esophageal cancer cells, and lymphoma cells intensified TSA-induced cell death.[52–54] BCL2 inhibitors synergized with SAHA in squamous cell carcinoma[55] and leukemic cells.[56,57] Thus, the BCL2 family can be therapeutically targeted to potentiate HDI-mediated anticancer effects or to overcome HDI resistance.[58,59] Similarly, EGFR is also known to substantially increase the IC50 of SAHA for cell death in head and neck cancer cells.[60] The identification of anti-apoptotic genes and EGFR from our CRISPRs screen is not surprising and does not necessarily indicate that the BCL2 family or EGFR are direct targets of HDIs. Rather, they are likely generic modulators of the cellular responses triggered by HDI treatment and other chemotherapies. The lack of correlation between HDAC expression and sensitivity to HDI is consistent with several prior studies.[61–65] Loss-of-function screens using RNA interference or CRISPR/Cas9 knockout in mammalian cells in the presence of HDIs also failed to detect HDACs.[66,67] However, diffuse large B-cell lymphoma (DLBCL) cell lines with higher expression of HDACs tended to be more sensitive to TSA.[68] HDAC2 is among the gene signatures predicting sensitivity to HDIs, as identified by correlating drug response profiles of five pan-HDIs with transcriptomes of solid cancer cell lines.[69] To further address this question in an unbiased, comprehensive manner, we retrieved transcriptomic data from the Cancer Cell Line Encyclopedia (CCLE) database and drug response data for SAHA (vorinostat) and MS275 (belinostat) from the matched cell lines in the GDSC and CTRP databases. Compared to top genes with high correlation to the SAHA and MS275 drug response, HDACs did not show significant correlation, except for HDAC11, which is modestly and positively associated with the drug resistance to SAHA and MS275 (Supplementary Fig. S5).

HDAC enzyme activity is dispensable for the cytotoxic effects of FK228

The lack of evidence for the consistent involvement of HDACs in cancer or HDI responses in the above unbiased analyses led us to directly assess whether HDAC enzyme activity is required for HDIs' cytotoxic effects. Mutation of key catalytic residues of HDAC can have dominant-negative effects on enzyme activity without altering HDAC protein levels or protein-protein interactions.[70–72] For instance, HDAC1-H140A, HDAC2-H141A, and HDAC3-H134A resulted in over 80% reduction in overall HDAC enzymatic activity but retained the capacity to associate with multi-protein complexes comparable to their wild-type counterparts.[72] A similar HDAC2 mutant (HDAC2-H142A) did not affect its interaction with the Sin3A, NuRD, or CoREST corepressor complexes.[70] The Y298F mutation in HDAC3 impaired its enzyme activity but did not affect HDAC3 interaction with NCOR/SMRT.[16] HDIs also do not affect the protein interactions between HDAC and its coregulators.[73] These findings suggest that the catalytic activity of HDACs is separable from their interaction with the multi-subunit corepressor complexes. Given the substantial workload required to suppress all HDACs simultaneously, we focused on Class I HDACs (HDAC1, 2, 3, and 8) and compared the effects of Class I HDACs-YF overexpression with those of Class I-specific HDIs (FK228 or MS275). We first confirmed that the HDAC YF mutants show a dominant-negative effect when co-expressed with wild-type (WT) HDACs in HEK293 cells, followed by immunoprecipitation and a fluorescence-based HDAC assay (Fig. 3a, b and Supplementary Fig. S6a). We found similar effects in AML12 and KP4 cells (Supplementary Fig. S6b, c). The dominant-negative effect does not need to fully abolish HDAC-WT enzymatic activity for this experiment, as HDIs do not necessarily need to completely abolish HDAC activities to exert cellular effects.

We then used adenovirus to express HDACs-YF or the GFP control, which can achieve nearly 100% infection efficiency in AML12 and KP4 cells after transient infection (Fig. 3c). The overexpression of Flag-tagged HDACs-YF mutant proteins was confirmed using immunoblot with individual HDAC antibodies (Fig. 3d and Supplementary Fig. S7a). Interestingly, exogenous HDAC2-YF expression appeared to be self-limiting, as endogenous HDAC2 levels decreased upon exogenous HDAC2 overexpression, suggesting tight autoregulation of HDAC2 protein abundance. YF

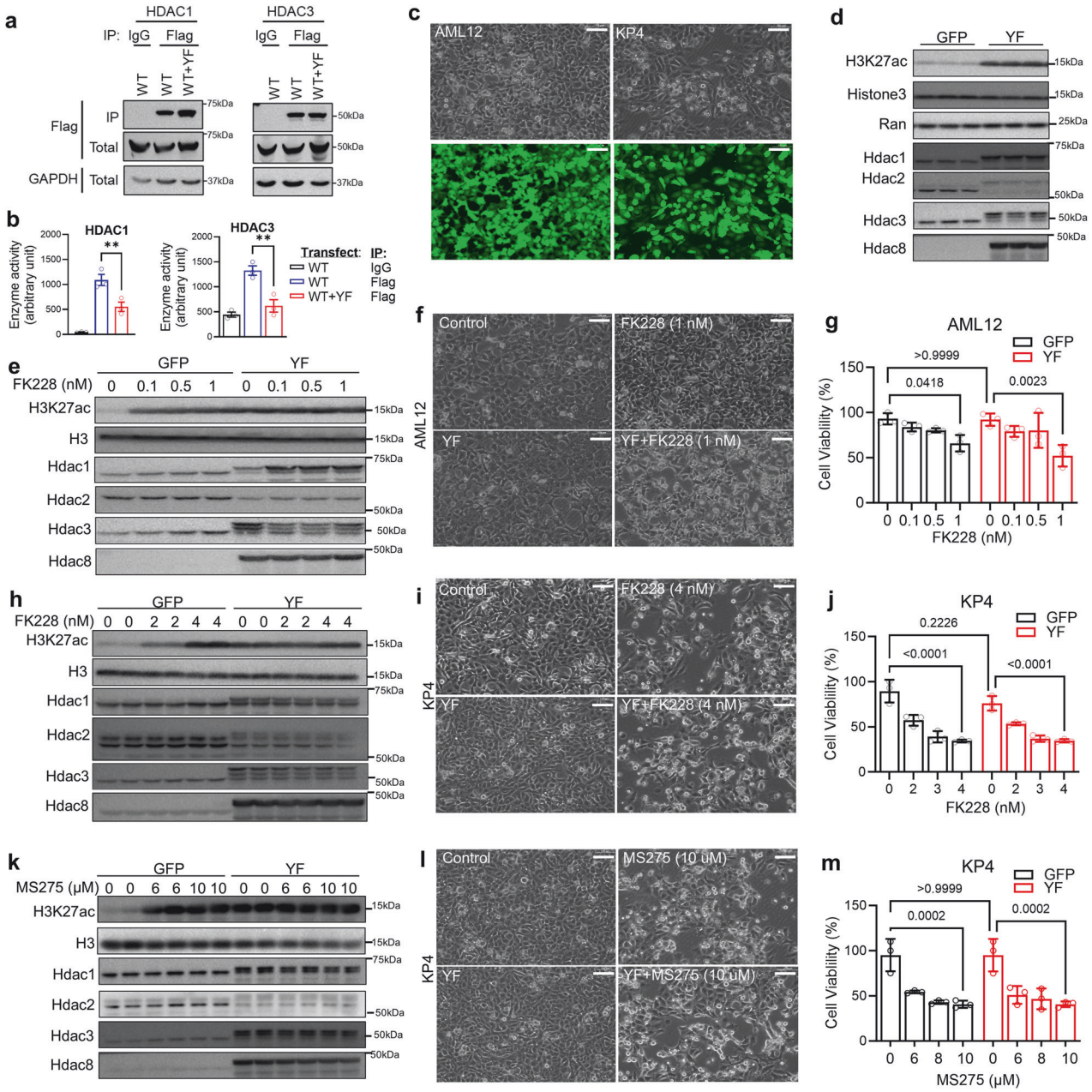

Fig. 3 The cytotoxic effects of FK228 and MS275 do not require the catalytic activity of Class I HDACs. **a**, **b** Immunoblot (IB) and fluorescence-based HDAC enzyme assay in the immunoprecipitates (IP) with normal IgG or anti-Flag antibodies from transfected HEK293 cells overexpressing the indicated Flag-tagged HDAC1,HDAC8 or HDAC3 wild-type (WT) and YF mutants at a 1:2 ratio. Data are mean ± SEM of three independent experiments. Analyzed by 1-way ANOVA and Tukey tests. **c** Brightfield and fluorescence microscopy of AML12 and KP4 cells infected with adenovirus expressing GFP(Scale bar:100 μm). **d** Immunoblot of HDACs, H3K27ac, and H3 in AML12 cells overexpressing HDAC1/2/3/8 YF mutants. **e** Immunoblot of HDACs, H3K27ac, and H3 in AML12 cells treated with FK228, with or without HDAC1/2/3/8 YF mutants overexpression. **f** Brightfield microscopy of AML12 cells after adenoviral-mediated overexpression of HDAC1/2/3/8 YF mutants and/or FK228 treatment(Scale bar:100 μm). **g** CCK-8 viability assay of AML12 cells as treated above. **h** Immunoblot of KP4 cells treated with FK228, with or without HDAC1/2/3/8 YF overexpression. **i** Brightfield microscopy of KP4 cells as described above, with FK228 treatment(Scale bar:100 μm). **j** CCK-8 viability assay of KP4 cells as treated above. **k** Immunoblot of KP4 cells treated with MS275, with or without HDAC1/2/3/8 YF mutants overexpression. **l** Brightfield microscopy of KP4 cells, as described above, using MS275 treatment(Scale bar:100 μm). **m** CCK-8 viability assay of KP4 cells as treated above. Data are mean ± SD of three independent experiments for CCK8 assays. Analyzed by 2-way ANOVA and Tukey's tests. ns not significant. *p*-values are as indicated

overexpression caused global elevation of H3K27ac compared to the GFP control (Fig. 3d), validating the dominant-negative effects on the endogenous protein targets of HDACs. We adjusted the dosages of the YF virus and HDIs to achieve similar levels of global histone hyperacetylation. Specifically, we added FK228 24 h after viral injection, harvested some cells 24 h later for immunoblot, and tested cell viability with CCK-8 and microscopy after another 48 h. We adjusted the virus dosage to lower the YF expression level so that it causes similar global H3K27 hyperacetylation as FK228 at 0.5-1 nM in AML12 cells (Fig. 3e and Supplementary Fig. S7b) but did not cause cytotoxicity (Fig. 3f, g). FK228 caused cytotoxicity regardless of YF overexpression (Fig. 3f, g). Similar results were

obtained in KP4 cells, where global histone acetylation was elevated by YF overexpression to levels comparable to those induced by FK228 or MS275 treatment, without causing obvious cytotoxicity (Fig. 3h–m). HDIs induced dose-dependent cytotoxicity irrespective of the presence or absence of YF mutants (Fig. 3h–m and Supplementary Fig. S7c, d). Although FK228 may not effectively inhibit HDAC3 or HDAC8, we chose to inhibit all Class I HDACs (HDAC1/2/3/8) as a fail-safe strategy, considering that HDACs may compensate for one another.[74] Thus, the observation that simultaneous blockade of HDAC1/2/3/8 enzymatic activity through YF overexpression neither reproduces the effects of Class I-specific HDIs nor interferes with HDI-induced responses suggests that HDIs do not act primarily through HDACs in the tested context.

The majority of transcriptomic effects of FK228 are independent of histone hyperacetylation

To compare the transcriptomic effects of FK228 and HDAC1/2/3/8 YF mutants overexpression, we performed RNA-seq in AML12 cells at 24 h after FK228 treatment in 4 groups: control, FK228 (FK), YF overexpression, and FK228 in combination with YF overexpression (FK + YF). Differentially expressed genes (DEGs) between the control group and any of the other 3 groups were identified using the standard cutoff criteria Log_2(Fold-Change)>1 and $q < 0.01$ (Fig. 4a–c). FK228 treatment upregulated 11-fold more genes (914 vs. 77) than YF overexpression, with 58 overlapping genes (Fig. 4a). Only 6.5% of FK228-activated genes were recapitulated by YF overexpression. A combination of FK228 and YF overexpression upregulated 1,614 genes (Fig. 4a). Similar results were obtained for downregulated genes, with FK228 downregulating far more genes than YF overexpression (Fig. 4b). HDI-unique genes are 15-fold more than YF-unique genes (1,767 vs. 116) and 4-fold more than the shared genes (1,767 vs. 393) (Fig. 4c). While HDI-unique DEGs were involved in various cancer-related pathways (Fig. 4d), shared DEGs (by both HDI and YF) were not enriched in cancer-related pathways (Fig. 4e). Many genes involved in cell proliferation were altered by FK228 but not by YF overexpression (Fig. 4f and Supplementary Table S6).

We further performed H3K27ac ChIP-seq to assess loci-specific histone acetylation on the chromatin. We chose H3K27ac as the primary readout of HDAC activity because it shows broader enrichment in both enhancers and promoters than H3K9ac. Prior study showed that H3K27ac and H3K9ac showed highly correlated changes in response to TSA,[75] which we confirmed by re-analyzing their dataset (Supplementary Fig. S8). FK228 treatment and YF overexpression led to an overall elevation in H3K27ac levels at transcription start sites (TSS) and transcription end sites (TES) of all genes, while combining FK228 with YF overexpression further increased chromatin-associated H3K27ac levels (Fig. 4g). After integrating DEGs (FK vs. control or YF vs. control) from the RNA-seq, we observed a similar pattern of H3K27ac levels across the gene bodies of all detectable genes (Fig. 4h). Since the liver HDAC3 ChIP-seq data are available,[76] we also focused on HDAC3 binding sites and observed similar patterns of H3K27ac level across groups (Fig. 4i). We also obtained similar patterns by focusing on other enhancer markers, such as EP300 or POLR2A binding peaks, or enhancers as defined by EnhancerAtlas2.0[77] (Supplementary Fig. S9). When we focus on genes, the pattern remains the same regardless of whether we focus on genes upregulated by both FK and YF, downregulated by both FK and YF, upregulated in FK but not YF, or downregulated in FK but not YF, POLR2A, as compared to the control, or even unchanged genes (Fig. 4j). Thus, histone acetylation patterns do not predict gene expression, suggesting that histone acetylation is insufficient to drive transcription activation.

We also examined whether HDI alters acetylation levels at genes identified in the CRISPRa library screen. Although FK228 elevated histone acetylation on most genes, there was no significant correlation between FK228-induced histone hyperacetylation and the fold-change enrichment of the genes in the CRISPRa library screen, indicating that HDI treatment does not significantly affect acetylation levels at genes identified in the CRISPRa screen more than those genes that were not enriched (Supplementary Fig. S10). In summary, most of the transcriptomic effects of FK228 were not recapitulated by YF overexpression despite their similar levels of histone hyperacetylation.

HDAC enzyme activity is dispensable for the in vivo anticancer effects of FK228

To address whether the in vitro results would hold up in vivo, we adapted an in situ liver cancer mouse model by transposon-based oncogenes.[78] We used β-catenin, c-Met, and c-Myc, whose dysregulation is strongly associated with human hepatocellular carcinoma.[79–81] Notably, c-Met is overexpressed in 20–48% of human HCCs, approximately 20% of cases harbor concurrent c-Met and β-catenin activation, and c-Myc is overexpressed in up to 70% of HCC.[79–81] Tumors generated using this system also recapitulate histopathological features observed in human HCC, including nodular and diffuse growth patterns.[82] We transduced transposon-based plasmids expressing c-Met, β-catenin, c-Myc, and a luciferase reporter into the mouse liver with or without HDAC1/2/3/8-YF plasmids through hydrodynamic tail vein injection. We chose FK228 for this in vivo study due to its higher potency than MS275. After 7 days, FK228 was i.p. injected three times a week until mice were imaged for luciferase at 5 weeks after hydrodynamic injection, followed by tissue harvest (Fig. 5a). HDI treatment, but not YF overexpression, efficiently reduced luciferase activity (Fig. 5b, c), liver weight (Fig. 5d), and liver size (Fig. 5e). H&E staining revealed extensive tumor cell infiltrate in the control group, which was diminished after HDI treatment, accompanied by necrosis and inflammatory infiltrate (Fig. 5f, g). YF overexpression did not change these morphological features or affect the FK228 effects (Fig f, g). Immunostaining analysis showed a similar level of H3K27 hyperacetylation in the FK and YF groups, which was potentiated in the YF + HDI group (Fig. 5h–i). FK228 reduced the expression of several tumor markers or proliferation markers regardless of YF overexpression (Fig. 5j). These data suggest that the in vivo anticancer effects of FK228 are independent of its HDAC-inhibiting activity.

Chemical modification of HDIs dissociates HDAC-inhibiting activity from anticancer effects

To test whether pan-HDIs require HDAC-inhibiting activity for their anticancer effects, we focus on SAHA, an approved pan-HDI. SAHA has a hydroxamic zinc-binding group (ZBG), which is crucial for chelating the zinc ion at the active site of HDACs. Switching the hydroxamic group to methyl or *t*-butyl esters reduced the HDAC-inhibiting activity.[83] Modification of the hydroxamic group can also lead to an 800- to 5000-fold decrease in HDAC-inhibiting activity.[84] Docking studies showed that the reduced potency of the modified SAHA analogs was due to fewer interactions with the catalytic pocket and a disrupted orientation.[85] These studies emphasize the importance of the hydroxamic ZBG in inhibiting HDAC. However, it was unknown how these modifications change the anticancer effects of SAHA. We chemically modified the ZBG of SAHA by removing the amide, yielding suberanilic acid (SAA) (Fig. 6a and Supplementary Fig. S11a). SAHA has an IC50 of 80 nM for inhibiting HDACs in the HeLa nuclear extracts, as determined by a fluorescence HDAC enzyme assay. By comparison, SAA did not show HDAC-inhibiting activity even at > 10,000 nM (Fig. 6b). The loss of HDAC-inhibiting activity in SAA was further confirmed by the absence of global H3K27 hyperacetylation, alpha tubulin acetylation, or SMC3 acetylation in MC38 cells when treated with SAA at the same or higher dosages than SAHA (Fig. 6c and Supplementary Fig. S11b, c).

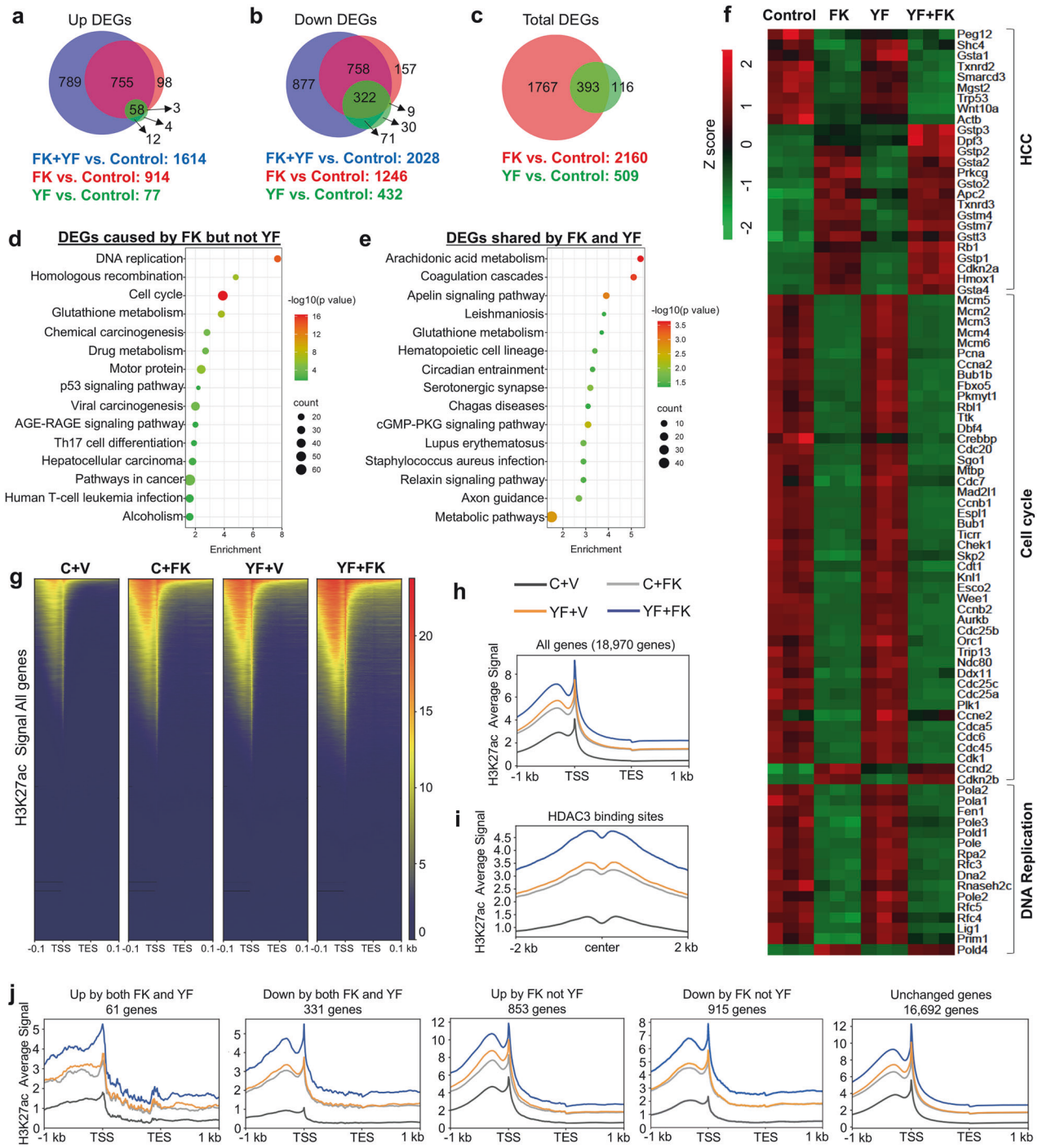

Fig. 4 The transcriptomic effect of HDI is independent of HDAC enzymatic activity. **a–c** Venn diagram showing the overlap of differentially expressed genes (DEGs) for the three indicated comparisons in AML12 cells, with $q < 0.01$ and |Fold-change | ≥ 1. **d**, **e** Dot plot of the enriched biological pathways of the indicated DEGs. **f** Heat map of gene expression levels for cancer-related DEGs across all four groups. **g** Heat map of H3K27ac ChIP-seq signal intensities across the transcription start sites (TSS) and transcription end sites (TES) on all genes for the 4 groups: C-GFP control, V-vehicle treatment, FK-FK228 treatment, YF-HDAC1/2/3/8 YF mutant overexpression. **h** Average H3K27ac ChIP-seq signal on the gene bodies across all genes. **i** Average H3K9ac ChIP-seq signals, represented by reads per bp in 10 million total reads, at the HDAC3 binding sites. **j** Average H3K27ac ChIP-seq signal at the gene bodies of the indicated subsets of DEGs

We then used a subcutaneous allograft mouse model to assess the anticancer effects of SAA and SAHA. MC38 is a well-characterized, immunocompetent syngeneic tumor model derived from C57BL/6 mice. MC38 tumors share key histological and therapeutic response features with human colorectal cancers and are widely used for in vivo evaluation of anticancer agents, including HDIs.[86,87] This model offers several advantages: (i) reproducible tumor growth kinetics in an immunocompetent host, enabling evaluation of both direct tumor cell effects and potential immune-mediated mechanisms;[88] (ii) established sensitivity to epigenetic modulators,[89] and (iii) compatibility with mechanistic studies such as pharmacodynamic biomarker analysis and

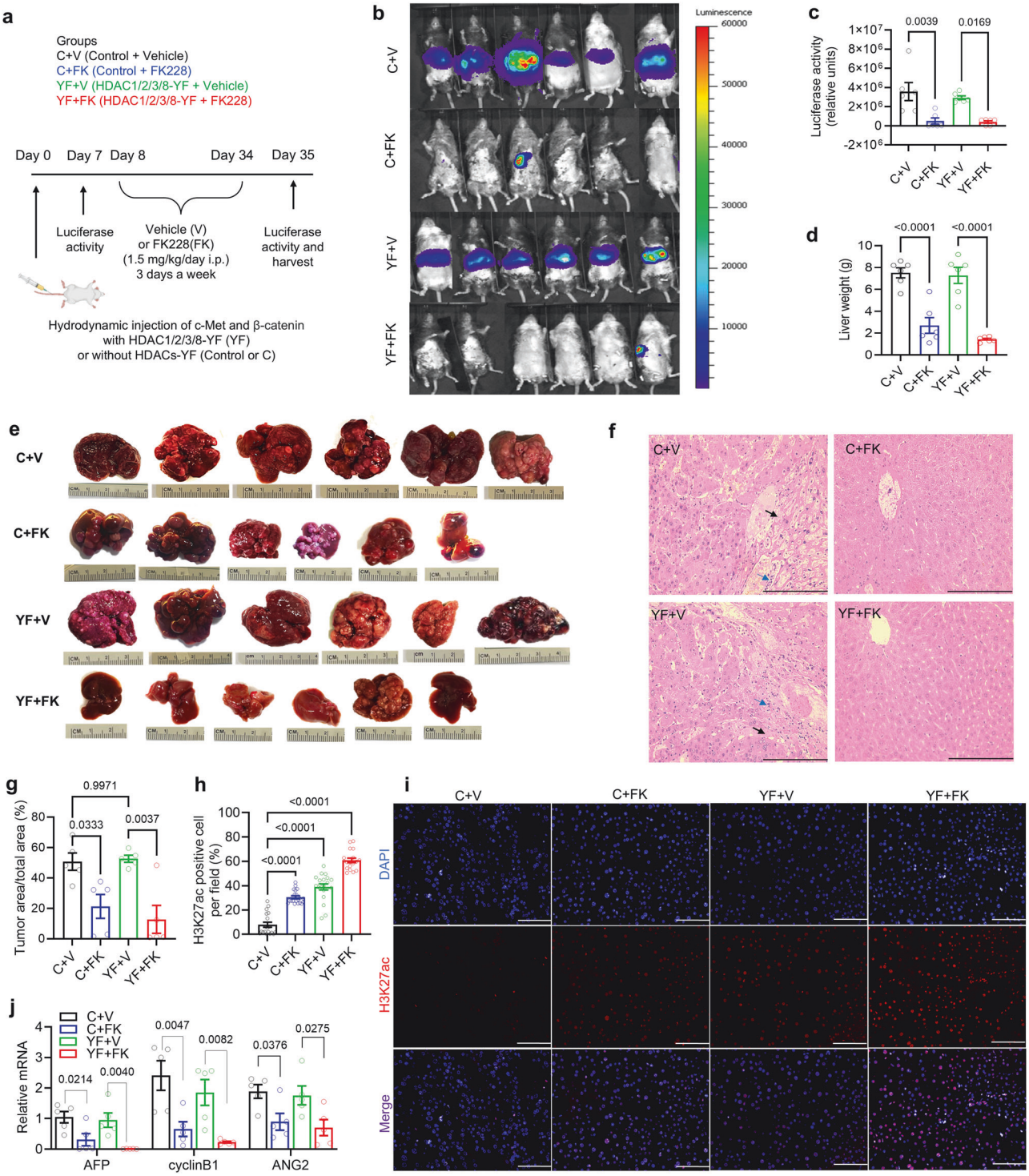

Fig. 5 HDAC enzyme activity is dispensable for the in vivo anticancer effects of FK228. **a** Experimental design for evaluating the efficacy of FK228 in a liver cancer mouse model induced by hydrodynamic injection of transposon-based plasmids expressing oncogenes c-Met and β-catenin. **b**, **c** In vivo imaging of luciferase activity and quantification at Day 35. **d** Weight of harvested liver. **e** Gross liver images. **f**, **g** H&E staining of liver tissue and quantification. Black arrows indicate necrotic regions. Blue arrows indicate inflammatory cell infusion. Scale bar:200 μm **h**, **i** H3K27ac immunofluorescence staining of liver tissues. Bar graph showing the quantification of the intensity of H3K27ac ($n = 20$ fields from 5 mice per group, Scale bar:100 μm). **j** RT-qPCR analysis of livers for the indicated HCC marker genes. Data are mean ± SEM. Data from individual mice were shown. Analyzed by 1-way ANOVA and Tukey's tests. ns not significant. *p*-values are as indicated

combination therapy testing.[90] Therefore, we selected the MC38 allograft as a preclinical model for assessing the antitumor potential of SAA. MC38 cells were injected subcutaneously into the right flank of adult C57BL/6 J mice, and the animals were allowed to recover from the surgery before being treated with vehicle, SAHA, or SAA at 50 mg/kg dosage daily for 19 consecutive days (Fig. 6d). SAHA and SAA caused a notable, similar decrease in tumor volume, as measured by caliper (Fig. 6e), without altering

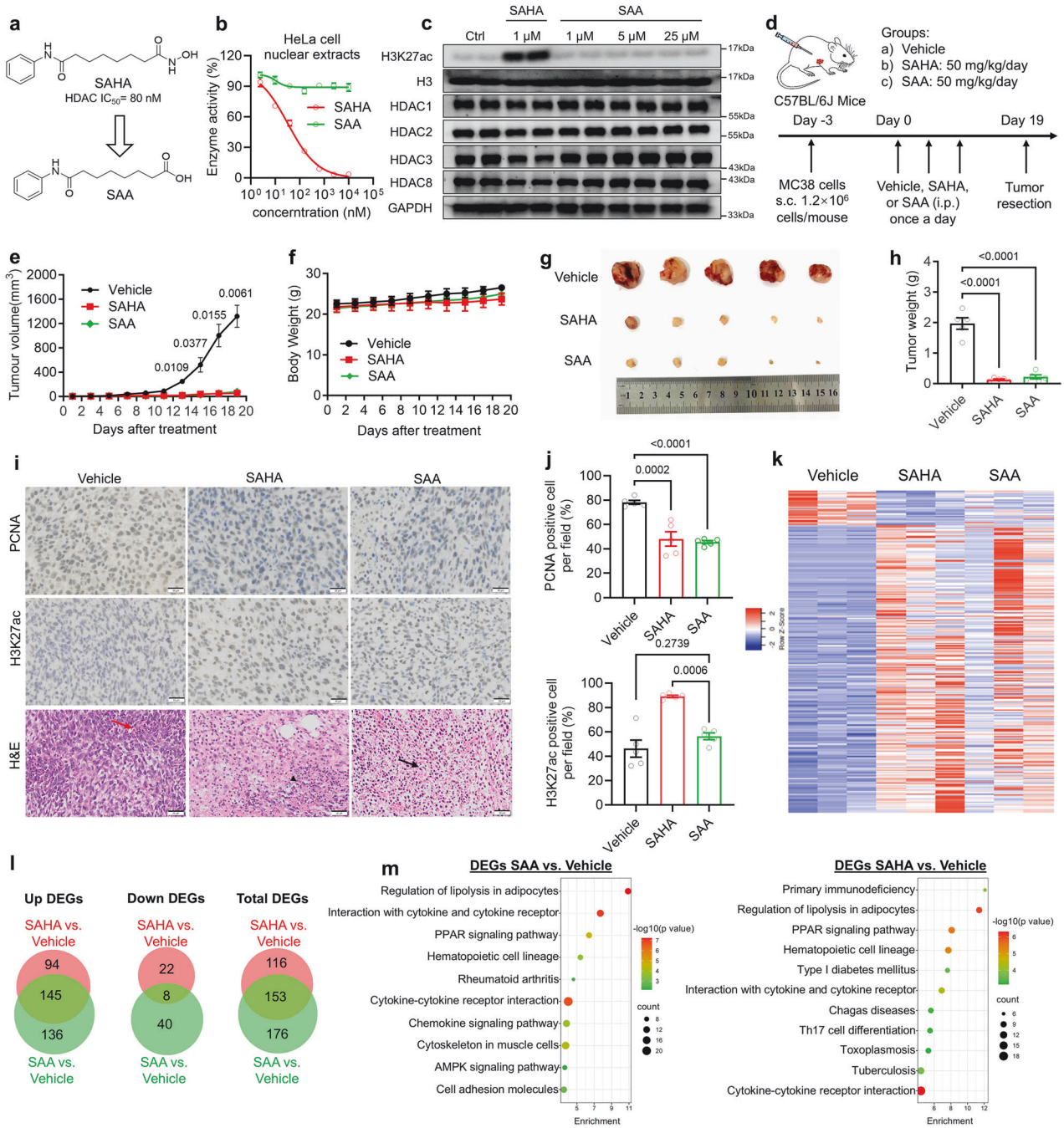

Fig. 6 Chemical modification of HDIs dissociates HDAC-inhibiting activity from anticancer effects. **a** Structure of SAHA and SAA. **b** Suppression % of the HDAC enzyme activity in HeLa nuclear extracts by SAHA or SAA. Data are mean ± SEM from technical triplicate. **c** Immunoblot of MC38 cells treated with SAHA or SAA. **d** Experimental design for evaluating the efficacy of SAHA and SAA in mice transplanted with MC38 cells. **e** Tumor volume calculated from caliper measurements (Volume = 0.5 × Length × Width²). Data are mean ± SEM. $n = 5$ mice. Analyzed by repeated 2-way ANOVA and Bonferroni's tests. **f** Body weight. Data are mean ± SD. **g**, **h** Gross pictures and weight of harvested tumors. Data are mean ± SEM. Analyzed by 1-way ANOVA and Tukey's tests. **i**, **j** H&E staining and immunohistochemistry analysis of PCNA and H3K27ac of the harvested tumors. Data are mean ± SEM. $n = 5$ mice. Analyzed by 1-way ANOVA and Tukey's tests. Scale bar: 50 μm. **k** Heat map of expression levels of DEGs (SAHA vs. vehicle) by RNA-seq analysis of tumors across all three groups ($n = 3$ mice). **l** Venn diagram comparison of SAHA-induced DEGs and SAA-induced DEGs in harvested tumors. **m** Dot plot of the top enriched pathways in DEGs caused by SAHA and SAA. *p*-values are as indicated

body weight (Fig. 6f). At the end of the experiment, tumors were harvested and weighed. SAHA and SAA both reduced the tumor weight by about 10-fold compared to the vehicle control (Fig. 6g, h).

Immunostaining showed a significant decrease in the proliferating cell nuclear antigen (PCNA) levels in the tumor after SAHA or SAA treatment compared to the vehicle control (Fig. 6i, j). H3K27ac levels were elevated by SAHA compared to the control, but not by SAA (Fig. 6i, j). Immunohistochemistry also confirmed that tubulin acetylation was robustly upregulated by SAHA but not by SAA (Supplementary Fig. S11d). Compared to the vehicle control, fewer tumor cells were found in the SAHA or SAA groups, which were

associated with extensive necrosis (black arrow) and inflammatory cell infiltration (black arrowhead). In contrast, the control group showed prominent tumor growth (red arrow) and minimal presence of inflammatory cells (Fig. 6i). RNA-seq analysis of the tumors identified differentially expressed genes (DEGs) among the 3 groups using the standard cutoff criteria Log_2(Fold-Change)>1 and q-value < 0.05. A clustered heat map of DEGs (SAHA vs. vehicle) shows that SAA and SAHA induced a similar overall pattern of transcriptomic changes (Fig. 6k and Supplementary Fig. S11e). Compared with vehicle control, SAHA led to 269 DEGs, while SAA led to 329 DEGs, with 153 overlapping genes, mostly upregulated (Fig. 6l). Pathway analysis showed that both SAA and SAHA regulate genes in lipid metabolism, immune response, and cell adhesion (Fig. 6m and Supplementary Table S7). These results suggest that the anticancer effects and transcriptomic outcome of SAHA are largely independent of its HDAC-inhibiting activity.

DISCUSSION

Five pieces of evidence suggest that HDAC enzyme activity is not necessarily the *de facto* target of HDIs in anticancer therapies. (1) Unbiased bioinformatics analyses found that genetic variants or expression levels of HDACs do not correlate consistently with most cancers or cancer patient survival. (2) Unbiased CRISPR library screens did not identify HDACs as genes affecting cellular responses to HDIs (SAHA or MS275). (3) Overexpression of dominant-negative, catalytically inactive Class I HDACs (HDAC1, 2, 3, and 8) caused similar histone hyperacetylation as Class I-specific HDI (FK228 or MS275) in cancer cell lines but did not cause similar cytotoxic or transcriptomic effects. (4) The anticancer effects of FK228 were independent of its HDAC-inhibiting activity in an in-situ liver cancer mouse model. (5) Chemical manipulations of a pan-HDI, SAHA, can abolish HDAC-inhibiting activity but retain most anticancer effects in a mouse allograft colon cancer model. Therefore, although some HDIs may still act through HDACs in certain contexts, our results suggest that this mechanism is not as generalizable or universal as previously assumed.

Although seemingly counterintuitive, our conclusion reconciles the inconsistencies between the universal anticancer effects of HDIs and the context-dependent tumor-suppressor role of HDACs. The possibility of non-HDAC targets for the anticancer effects of HDIs also resolves the discrepant transcriptomic effects of different HDIs.[13,15] Only 7 common DEGs were identified across SAHA, VPA, and TSA treatments, while each treatment altered 200–600 DEGs in HL60 cells.[15] SAHA and panobinostat shared only 11 genes in colon cancer cell lines.[91] Hydroxamic acid-based HDIs, CG-152 and TSA, led to distinct DEGs in LNCaP cells, with TSA regulating five times more genes involved in cell death and cell cycle than CG-152.[92] Therefore, transcriptomic effects of HDIs vary significantly among HDIs. Such a discrepancy in gene expression signatures among different HDIs suggests that they might exert their anticancer effects through distinct or transcription-independent mechanisms.[93,94]

Our results do not exclude the possibility that HDIs might indeed act through HDACs in certain cancer types. However, we want to apply the same standard of scientific rigor when evaluating the evidence supporting the argument that HDIs primarily exert their effects through HDAC inhibition. HDIs certainly inhibit HDACs, and the knockdown of specific HDACs can suppress certain cancers. But HDAC proteins are versatile and have enzyme-independent functions. In primary mouse hepatocytes, pan-HDIs failed to regulate the HDAC3-targeted lipogenic genes, in contrast to HDAC3 knockdown.[16] Similarly, blocking HDAC3 deacetylase activity with TSA and catalytic dead mutants did not affect HDAC3's carrier role in TR2/PML colocalization in embryonic stem cells.[95] Testis-specific HDAC3 knockout, but not HDAC3 catalytic activity inactivation, disrupted the expression of spermatogonial genes and reduced fertility.[96] The function of HDAC3 in embryonic development, cardiac development, and cardiac contraction is largely independent of its enzyme activity.[97–101] HDAC2 was shown to activate expression of some genes in a deacetylase-independent manner.[102] Inhibition of HDAC7 by TSA was insufficient to abolish HDAC7-mediated repression of Runx2 activity.[103] Thus, the loss of HDAC enzyme activity does not replicate the effects of reduced HDAC protein level in many contexts. The fact that HDIs or HDAC knockdown can suppress cancer in some contexts does not demonstrate that HDIs act through HDACs, given that HDIs may interfere with other proteins, and that knockdown of many such proteins may suppress cancer. Therefore, it appears that the traditional view of HDIs exclusively targeting HDACs for all cancer types is an oversimplification. Instead, HDI-induced effects could stem from pathways independent of HDAC inhibition.

While numerous studies have investigated the correlation between HDIs and histone hyperacetylation, fewer have explored the role of histone hyperacetylation in cell growth or proliferation. Despite global histone hyperacetylation induced by HDIs in our study, only a small proportion (~9%) of genes across the genome showed transcriptional changes. These data demonstrate that H3K27ac levels are not a good marker of the anti-cancer effects of HDI, although they can be a good marker of HDAC-inhibiting effects. These results are consistent with the fact that less than 10% of the genes in the entire genome showed expression changes after TSA, VPA, or SAHA treatment in HL60 cells.[15] Similarly, the HDI suberic bishydroxamate (SBHA) did not inhibit cell growth despite inducing a comparable accumulation of hyperacetylated histones.[104] The pharmacological dissociation kinetic rates of HDIs do not necessarily correlate with their cellular or transcriptomic effects.[12] These results suggest that the growth inhibition or cell death triggered by HDIs occurs through mechanisms independent of their effects on global histone acetylation.

If not histone hyperacetylation, what could be the target for HDIs for their growth-inhibiting activity? One obvious possibility is non-histone targets. Many non-histone targets, such as cell cycle regulators, transcription factors, and other structural proteins, are involved in different cell cycle stages. HDACs can regulate the cell cycle by deacetylating p53 and c-Myc, affect DNA damage responses by deacetylating BRCA1, or regulate other cellular processes by deacetylating proteins in the Wnt/β-catenin and Hedgehog pathways.[105] However, our experimental approaches using dominant-negative HDACs and chemical modification of HDIs directly alter the catalytic site or the interaction of HDIs with it, affecting both histone and non-histone substrates, including alpha-tubulin and SMC3, as tested. Thus, our results suggest that HDI-induced hyperacetylation on any protein can be dissociated from its anticancer effect.

Our unbiased analysis of large public databases did not find a consistent universal correlation between HDAC expression and cancer across all cancer types. These results contradict the literature reporting a positive correlation between HDACs and cancer. Several factors might contribute to such contradictions. (1) The correlation can be cancer-type specific. Consistent with our analysis, elevated HDAC1 expression is associated with lung cancer,[106] elevated HDAC11 expression is associated with hepatocellular carcinoma prognosis,[107] and decreased HDAC5 expression is correlated with poorer prognosis in breast cancer.[108] (2) Small patient cohorts limit many human studies. Utilizing the TCGA database, one of the largest repositories of cancer genomics data, our study provides a comprehensive assessment of HDAC-cancer correlations across 662 tumor-normal paired samples from 17 cancer types. (3) Non-significant results are less likely to be reported in the literature.

Our study has limitations. (1) Whether our conclusion is generalizable to other cell lines, cancer models, or cancer types other than those we tested is yet to be determined. We selected

liver, pancreatic, and colon cancer cells because they respond to HDIs and have readily available mouse models. (2) Since it is currently infeasible to cover all HDACs and all HDIs across all cancer types or cellular contexts for YF overexpression studies, we focus on Class I HDACs because they exhibit stronger enzymatic activity than Class IIa HDACs and are the classical targets of most HDIs. Thus, whether the conclusions extend to other HDACs and HDIs remains to be determined. However, Class I HDACs contribute to the enzymatic function of Class IIa HDACs.[5] Our chemical manipulation of SAHA, a pan-HDI, suggests that its effect is unlikely to be mediated by other HDACs in the context tested. (3) The true targets of HDIs remain elusive. Identifying the authentic molecular targets of HDIs represents an important next step that requires systematic, unbiased approaches. Our CRISPR library screen and omics profiling results, along with other omics profiling,[109] provide multi-omics resources for future endeavors toward this goal.

MATERIALS AND METHODS

TCGA mRNA expression and mutation data analysis

We obtained normalized gene expression data based on RNA-Seq by expectation maximization (RSEM) and mutation data in MAF (Mutation Annotation Format) files from the TCGA portal (http://gdac.broadinstitute.org/). HDACs, canonical oncogenes, and tumor-suppressor genes were considered differentially expressed between tumor and normal paired samples if the fold-change > 1.5 and t-test FDR < 0.05. The normal sample was taken from adjacent non-tumorigenic tissue in the same patient. A total of 662 tumor-normal paired samples from 17 cancer types were used in the DEG analysis. The sample size for each cancer type was provided in the supplementary tables. We employed a Cox model and a log-rank test to evaluate the association between HDAC expression and overall survival in cancer patients, with FDR < 0.05 considered statistically significant. The high- or low-expression group consists of samples with HDAC expression levels (RSEM) above or below the median in the TCGA cohorts (Top or bottom 50%), respectively. We filtered out samples with more than 1000 mutations in the exome to eliminate potential bias introduced by ultra-mutation samples. The number and frequency of non-silent somatic mutations were calculated per gene for each cancer type.

Drug response and gene correlation analysis

Cancer cell lines in the Cancer Cell Line Encyclopedia (CCLE) were categorized into two groups based on HDACs, BCL2L1, and EGFR gene expression (RNA-seq data). The drug sensitivities of the top 25% and the bottom 25% cancer cell lines in GDSC and CTRP were then compared using the Mann–Whitney U test.

Lentiviral CRISPR/Cas9 SAMv2 library screen

Human CRISPR activation (CRISPRa) library version 2 (SAMv2) and MS2-p65-HSF1v2 (lenti-MPHv2) were from Addgene (#1000000078). The SAMv2 plasmid consists of sgRNA with MS2 stem-loop and dCas9-VP64. Plasmids were packed in HEK293T cells using the virus packaging mixture (psPAX and pMDG). 48 h post-transfection with the packaging mixture, virus-containing media were harvested. Hep3B cells were first transduced with lenti-MPHv2 and selected with hygromycin (600 μg/ml) to establish an MPHv2-expressing Hep3B stable cell line. MPHv2-expressing Hep3B cells were then subjected to large-scale transduction with the single lentiviral vector expressing dCas-VP64 and sgRNA library. Hep3B cells were allowed to grow to 30–40% confluency before adding the virus at appropriate doses, along with polybrene (8 μg/ml), so that 30% of the cells were transduced. Blasticidin (10 μg/ml) was added to the cells 24 h post-transduction and maintained for 4 days with media change every 2 days to select transduced cells. Selection of SAHA- and MS275-resistant cells using the pooled Hep3B-SAM cell library was performed according to the protocol described in ref. [50]. Briefly, the pooled Hep3B-SAM cell library was treated with SAHA (2 uM), MS275 (4 uM), or vehicle control for 5 days, with media and drugs replenished every 2 days. A total of 350 million cells across 8 dishes (15 cm) were used for the screen, yielding 500 cells per sgRNA and 70,290 gRNAs. The dosage and duration of SAHA and MS275 treatment were determined by a series of optimizations targeting 90% cell death. Surviving cells were subjected to genomic DNA extraction. For the amplification and purification of candidate sgRNAs, the sgRNA coding regions were first PCR-amplified using primers containing appropriate overhangs for sequencing. The resulting PCR products were purified using a QIAquick PCR Purification Kit (Qiagen) according to the manufacturer's instructions. The purified DNA was quantified and then subjected to high-throughput sequencing. To analyze the sequencing data from the CRISPRa library screen, we used the CRISPRBetaBinomial algorithm, which quantifies read counts and identifies enrichment at both the guide and gene/isoform levels. We first quantified the read counts of 70,297 guides for each sample. We then performed normalization by calculating CPM (Count Per Million). After the normalization, we calculated the $\log_2$(Fold-Change) for each guide. Since multiple sgRNAs are designed to target each gene, we calculated the mean of all sgRNAs targeting the same gene to get the final $\log_2$(Fold-Change). As a result, $\log_2$(Fold-Change) was calculated for 18,869 genes. The experiment was conducted only once, considering the cost and the lack of HDAC gene enrichment for both SAHA and MS275.

Cells and chemicals

Hep3B, AML-12, and KP4 cell lines were cultured according to the protocol described by the supplier in their specific media supplemented with 5% heat-inactivated fetal bovine serum (FBS) (Fisher SH3007903) and 1% antibiotic-antimycotic solution (Gibco Co) at 37 °C in a 5% CO_2 atmosphere. MC38 colon carcinoma cell lines were cultured in Iscove's Modified Dulbecco's Medium (ATCC, 30-2005) containing 8% FBS, 2 mM L-glutamine, and 50 μM beta-mercaptoethanol. SAHA (Sigma, SML0061), MS275 (AdooQ bioscience, A10611), and FK228 (MCE, HY-15149) were obtained from the indicated commercial sources.

DNA, virus, and cellular assay

To overexpress BCL2 family genes in Hep3B cells, human BCL2L1, BCL2, and BIM (cDNA from Genescript) along with a Flag tag were cloned into pCW57.1-T2A-GFP (Addgene #100521),[110] a Tet-Off lentiviral expression vector. A self-cleaving T2A peptide was incorporated downstream of BCL2 to enable the bicistronic expression of GFP as a separate protein, allowing fluorescence-based tracking of BCL2 expression. The final constructs, including pCW57.1-BCL2-flag-T2A-GFP, pCW57.1-BCL2L1-flag-T2A-GFP, and pCW57.1-BIM-flag-T2A-GFP, were verified by Sanger sequencing to confirm correct insertion and reading frame integrity. For lentivirus production, HEK293T cells were plated in a 10 cm dish and allowed to attain 60-80% confluency. A plasmid mixer was prepared and transfected into the cells using Lipofectamine. The culture medium from the transfected cells was collected after 48 h, centrifuged, and filtered through 0.45 μm filters. The resultant crude viral lysates were used to transduce Hep3B cells to generate stable cell lines. Hep3B cells were transduced with viral lysates for BCL2, BCL2L1, or BIM in the presence of 8 μg/mL polybrene. After 24 h, transduced cells were selected with 1 μg/mL blasticidin for 3 days in the presence of 1 μg/mL doxycycline. Subsequently, cells were seeded into 96-well plates at 100 μL per well in a complete medium supplemented with 1 μg/mL doxycycline. Once cells reached approximately 30–40% confluency, they were treated with SAHA (1 μM) or MS275 (2 μM) in the presence or absence of doxycycline. After 24–48 h of drug treatment, fluorescence and brightfield microscopy (Leica DMi8) were used to check for GFP

expression and cell morphology. After 3–4 days of HDIs treatment, Cell Counting Kit-8 (CCK-8) reagent was added to each well and incubated for 2 hours at 37 °C. Absorbance was measured at 450 nm to assess cell viability.

For overexpressing HDACs in AML12 and KP4 cells, human HDAC cDNAs were subjected to site-directed mutagenesis to generate HDAC YF mutants, which were subsequently cloned into the pENTR and pAd-CMV adenoviral gateway vector (ThermoFisher Scientific), driven by the CMV promoter for robust expression. The final constructs include pAd-CMV-HDAC1-Y303F-Flag, pAd-CMV-HDAC2-Y304F-Flag, pAd-CMV-HDAC3-Y298F-Flag, pAd-CMV-HDAC8-Y306F-Flag, and pAd-CMV-GFP as the control. For adenoviral production, the adenoviral plasmids were linearized and transfected into HEK293A cells following the instructions of the ViraPower™ Adenoviral Expression Systems (ThermoFisher Scientific). After the cytopathic effect was observed, the crude viral lysates were harvested by freezing and thawing the cell lysates, followed by centrifugation and filtration to remove debris. For adenoviral overexpression of YF-mutant HDAC in AML12 and KP4 cells, cells were seeded to reach approximately 60–70% confluency at the time of infection. Cells were then incubated with the crude viral lysates for 4 hours. The dosage of the crude cell lysates was optimized by visualizing GFP, so that almost all cells were transduced after 12 h of infection. After 4 h of infection, the viral medium was replaced with fresh complete-growth medium. HDIs were added 24 h post-transfection. For western blotting, cells were harvested 24 h after HDI treatment, and for the cell viability assay with Counting Kit-8 (CCK-8), cells were harvested 3 days after the start of HDI treatment.

Western blot, immunoprecipitation, and HDAC assay

Proteins were extracted from AML12 or KP4 cells or liver tumor tissues using RIPA buffer (150 mM NaCl, 1.0% IGEPAL® CA-630, 0.5% sodium deoxycholate, 0.1% SDS, 50 mM Tris, pH 8.0) supplemented with protease and phosphatase inhibitors. Cells and tissue samples were homogenized in RIPA buffer and centrifuged. The protein-containing supernatant was collected, and its concentration was measured using the BCA reagent (Thermo Scientific). The samples were denatured in a sampling buffer at 95 °C for 10 min. A total of 30 µg of protein was loaded onto SDS–polyacrylamide gels, and western blotting was performed with antibodies against HDAC1 (Abcam #7028), HDAC2 (Abcam #32117), HDAC3 (Santa Cruz #11417), HDAC8 (Abcam # 87139), H3K27ac (Abcam #4729), H3 (Abcam #1791), Flag (CST #D6W5B), and GAPDH (Abcam #14C10). Images were acquired using LumiQuant AC600 (Acuronbio Technology Inc). Quantification analysis was performed using ImageJ software. For protein extraction from MC38 cells, similar procedures were used with antibodies for H3 (Cell Signaling Technology, 4499 T), H3K27ac (Abways, CY9439), SMC3 (ABclonal, A19591), Ac-SMC3 (Sigma-Aldrich, MABE1073), α-Tubulin (ABclonal, AC012), Ac-α Tubulin (ABclonal, A24738) HDAC1 (Abmart, T55154S), HDAC2 (Abmart, T55062S), HDAC3 (UpingBio, YP-Ab-01762), HDAC8 (UpingBio, YP-Ab-01768), and GAPDH (Abways, OX9YYF111510).

For immunoprecipitation and HDAC assay, HEK293 cells were seeded in 6-well plates. Two wells were transfected with a Flag-tagged HDAC wild-type (WT) plasmid, while one well was co-transfected with both the Flag-tagged HDAC WT and mutant constructs. Cells were lysed 48 h after transfection in lysis buffer containing 20 mM Tris-HCl (pH 7.5), 150 mM NaCl, and 1% NP-40, supplemented with a protease inhibitor cocktail. Lysates were first pre-cleared with Protein G agarose beads, followed by incubation with anti-Flag M2 beads (Sigma A2220) or IgG control (CST #2729S) plus Protein G beads. Immunoprecipitates were washed three times with the lysis buffer (1% NP-40) to remove nonspecific interactions. The bead-bound immunoprecipitates were then subjected to HDAC enzymatic activity assays (Cayman 10011563) following the manufacturer's instructions. The reaction was initiated by adding the fluorogenic substrate and incubating at 37 °C for 30 min. After substrate deacetylation, the developer solution was added, and the mixture was incubated for an additional 15 min. Fluorescence intensity was measured using a plate reader at 360 nm excitation and 465 nm emission. For the HDAC assay with HeLa nuclear extracts, 50 µL of test compounds SAHA and SAA solutions with gradient concentrations were added in a 96-well black microplate, followed by 10 µL of pre-chilled diluted HeLa nuclear extract (Enzo, BML-KI140-0100). The mixture was pre-incubated at 4 °C for 5 min. Subsequently, 40 µL of the substrate (Boc-Lys(Ac)-AMC, synthesized in-house) was added to each well, followed by incubation at 37 °C on a thermostatic shaker for 30 min. The reaction was terminated by adding 100 µL trypsin stop solution (Solarbio, T8150) to each well. Fluorescence intensity was measured using a microplate reader (excitation wavelength 390 nm/emission wavelength 460 nm). Experimental controls included a 100% enzyme activity control group (using an equivalent volume of HDAC buffer instead of the test compounds) and a blank control group (replacing both the test compounds and the nuclear extract with HDAC buffer). The enzyme inhibition rate at each concentration was calculated based on relative fluorescence intensity, and IC50 values were determined through regression analysis using GraphPad Prism.

Mice, hydrodynamic injection, and luciferase assay

Animal procedures were approved by the Institutional Animal Care and Use Committee (IACUC) of Baylor College of Medicine in accordance with the NIH Guide for the Care and Use of Laboratory Animals or Shandong University in China. All mice were housed under a 12 h light/ 12 h dark cycle. Adult male C57BL6/J mice at 6–9 months old were used for the experiment. Plasmids used in the hydrodynamic injection include pT3-EF1a-cMet (Addgene #86498),[111] pT3-EF1a-N90-beta-catenin (Addgene #86499),[111] pCMV(CAT)T7-SB100 (Addgene # 34879),[112] and pT3-Myc-IRES-Luc (Addgene # 129775).[113] pT3-mCherry-NLS was made by cloning mCherry, a DsRed fluorescent protein monomeric derivative, into the pT3 vector backbone carrying EF1α promoter. A nuclear localization signal (NLS) sequence was fused to the C-terminus of mCherry to direct nuclear localization. Two HDAC YF mutants were cloned into one pT3 vector backbone carrying EF1α promoter. IRES (internal ribosome entry site) was inserted between the two consecutive HDACs for bicistronic expression. A bovine growth hormone (BGH) polyadenylation sequence was inserted through PCR, ensuring efficient transcription termination and mRNA stability. The final constructs for hydrodynamic injection of HDAC mutants were pT3-EF1-HDAC2 (Y304F)-IRES-HDAC1 (Y303F) and pT3-EF1-HDAC3 (Y298F)-IRES-HDAC8 (Y306F). All plasmids were prepared using endotoxin-free Maxiprep (Zymogen) according to the manufacturer's protocol. Mice were injected via hydrodynamic tail vein injection with a total of 51 µg of plasmids in saline. The total number of plasmids was kept equal between groups using the mCherry plasmid. The plasmids were diluted in saline to a volume equal to 9% of the mice's body weight and injected into the tail vein within 5 seconds. FK228 was started on Day 8 after hydrodynamic injection at 1.5 mg/kg three times a week. At 1 week and 5 weeks after the hydrodynamic injection, mice underwent luciferase activity imaging using IVIS Lumina X5 after receiving 3 mg/kg luciferin via intraperitoneal injection. The animals were euthanized through CO_2 asphyxiation at the end of the experiment for tissue harvest. For the allograft mouse model, MC38 cells at 80% confluency were diluted in PBS, and 1.2×10^6 cells were injected subcutaneously into the hind leg flank of adult C57BL/6 J mice. Mice were divided into three groups, and each group was intraperitoneally (i.p.) injected with either PBS, SAHA, or SAA at 50 mg/kg per day. Tumor volumes were calculated from tumor length and width measurements every other day (Volume $= 0.5 \times \text{Length} \times \text{Width}^2$). After 19 days of

treatment, the animals were sacrificed, and tumors and other organs were harvested in formalin or by snap freeze.

Immunofluorescence and immunohistochemistry

Tissue samples were fixed in 4% paraformaldehyde (PFA) in PBS overnight at 4 °C, then incubated in 15% and 30% sucrose in PBS at 4 °C until they sank. Samples were subsequently embedded in paraffin and sectioned at 6 μm thickness. For immunofluorescence staining, tissue sections were permeabilized with 0.1% Triton X-100 and 0.1% sodium citrate, then subjected to antigen retrieval and blocking. Sections were incubated overnight at 4 °C with primary antibodies against H3K27ac. After washing, slides were incubated with Alexa Fluor 594 goat anti-rabbit secondary antibody. For immunohistochemical staining, paraffin-embedded tissue sections were sequentially dewaxed with the dewaxing solution, anhydrous ethanol, and water. Antigen retrieval was performed using Tris-EDTA solution (Beyotime, P0084), followed by natural cooling and washing with water. Endogenous peroxidase activity was blocked with 3% hydrogen peroxide, and sections were further blocked with 3% BSA (Servicebio, GC305010) for 1 h at room temperature (RT). Samples were then incubated overnight at 4 °C with primary antibodies against PCNA (Abways, AB0051) and H3K27ac (Abways, CY9439). After washing, sections were incubated with HRP-conjugated secondary antibody at RT for 50 min, followed by visualization with freshly prepared DAB substrate (Servicebio, G1212). Nuclei were counterstained with hematoxylin and briefly treated with a differentiation solution. The sections were then dehydrated with graded ethanol, cleared with xylene, and sealed with neutral gum. For Hematoxylin-Eosin (H&E) staining, mouse tumor tissues were rinsed with cold PBS, fixed in 4% PFA (Servicebio, G1101), dehydrated, cleared, and paraffin-embedded. After sectioning, slides were dewaxed, rehydrated, and stained with hematoxylin and eosin (Solarbio, G1120). Differentiation was performed using 1% hydrochloric acid ethanol, followed by tap water rinsing, dehydration, clearing, and sealing with neutral gum (Solarbio, G8590). Stained sections were observed and imaged using a microscope. The tumor area was quantified from H&E-stained images by subtracting non-tumor regions. Staining intensity was quantified using ImageJ.

RT-qPCR, RNA-seq, and data processing

Total RNA was extracted from cells or tissues using TRIzol™ Reagent (Thermo Fisher Scientific, Waltham, MA, USA) according to the manufacturer's protocol. The concentration was analyzed using a Qubit™ RNA HS Assay Kit (Thermo Fisher Scientific, Waltham, MA, USA) in a Qubit Fluorometer (Thermo Fisher Scientific, Waltham, MA, USA). The purity and integrity of the RNA samples were determined in a Bioanalyzer 2100 system (Agilent Technologies, Santa Clara, CA, USA) using an Agilent RNA 6000 Pico Kit (Agilent Technologies, Santa Clara, CA, USA). For RT-qPCR, Applied Biosystems™ High-Capacity cDNA Reverse Transcription Kit (Fisher Scientific). For RNA-seq, the RNA samples were sequenced on the BGISEQ platform, generating about 6.56 Gb of data per sample in PE100 mode. The sequencing data were filtered with SOAPnuke (v1.5.2) by removing reads containing sequencing adapters, reads whose low-quality base ratio is more than 20%, and reads whose unknown base ('N' base) ratio is more than 5%. The average mapping ratio with the reference genome is 94.92%, and the average mapping ratio with the genes is 76.59%. A total of 19,037 genes were identified. The resultant clean reads were obtained and stored in FASTQ format and mapped to the reference genome GRCm38.p6 using HISAT2 (v2.0.4). Bowtie2 (v2.2.5) was used to align the clean reads to the reference coding gene set, and gene expression levels were calculated with RSEM (v1.2.12). The differential expression analysis was performed using DESeq2 (v1.4.5). GO and KEGG enrichment analyses of annotated differentially expressed genes were performed using DAVID Bioinformatics Resources 6.7. The z-score was calculated using the formula $z = (x-\mu)/\sigma$, where x is the FPKM value for each sample, μ is the population mean for all samples, and σ is the population standard deviation of all samples. RNA sequencing was performed on the tumor tissues of MC38 tumor-bearing mice. Total RNA was extracted from tumor tissues to determine purity and concentration. Qualified RNA samples were fragmented and reverse-transcribed into cDNA. RNA sequencing was performed using a high-throughput sequencing platform (Tsingke Biological Technology). The data undergoes quality control, comparative analysis, and bioinformatics processing to identify differentially expressed genes and transcripts between groups.

ChIP-seq and data processing

For ChIP, cells were homogenized and cross-linked in 1% formaldehyde for 20 min at room temperature. Whole-cell extracts were sonicated, followed by immunoprecipitation with antibodies for H3K27ac (Abcam, ab4729) and Protein A Sepharose CL-4B (GE, 17-0780-01). After the immunoprecipitation, beads were washed with ChIP dilution buffer (50 mM HEPES (pH 7.5]), 155 mM NaCl, 1.1% TritonX-100, 0.11% NaDeoxycholate, 1 mM EDTA) three times followed by a wash with ChIP wash buffer (50 mM Tris-HCl (pH 8.0), 10 mM EDTA, 0.5% NaDeoxycholate, 250 mM LiCl, and 0.5% NP-40). Sepharose beads were further washed once with TE buffer (Promega, E260A). DNA was enriched with phenol-chloroform extraction and dissolved in 20 μl TE buffer, followed by RNA degradation by RNase (Roche, 11119915001) for 30 min at 37 °C. For each treatment condition, three independent ChIP reactions, each from a separate plate of cells, were initially assessed by qPCR to evaluate variability. The reactions were then pooled and sequenced as a single sample for each treatment, along with the pooled total input DNA used as a control. The precipitated DNA was amplified according to the manufacturer's guide of Illumina (Illumina TruSeq ChIP Library Preparation Kit), followed by 50 bp single-end deep sequencing on Illumina Genome Analyzer IIx. The raw ChIP-Seq reads were trimmed with fastp v0.23.2 and aligned to the mouse reference genome (mm39) using bwa version 0.7.17-r1188. Only the uniquely mapped reads were retained. The bam files were sorted using Samtools version 0.1.19-44,428 cd. The peaks were called using macs2 version 2.2.7.1. The HOMER toolkit was used to produce BigWig files. The HDAC3 ChIP-seq binding sites are obtained from the Gene Expression Omnibus database (accession number GSE90533). The deepTools (version 3.5.1) was used to calculate the average signals around HDAC3 binding sites and gene transcription start/end sites from H3K27ac BigWig files of each ChIP-seq sample. The Log2 H3K27ac signal change is first normalized using log2(ChIP versus input ratio), then calculated by taking the normalized H3K27ac levels of the ±2k regions around genes' transcription start sites (for promoters) or integrated enhancer regions (for enhancer) from mouse liver obtained from EnhancerAtlas 2.0.[77] The EP300 and POLR2A binding peaks were obtained from the ENCODE project,[114] and the H3K27ac signal change was calculated as previously described. To compare the changes in H3K27ac and H3K9ac signals after HDI treatment in the Min6 beta cell line, we downloaded processed bigwig files from GSE234144. We selected genomic regions on a 10k window with upregulated H3K27ac (HDI vs vehicle, log2 Fold Change > 1) and examined H3K9ac changes (HDI vs vehicle) on the same regions. The FC calculation was performed using deeptools bigwigCompare (v3.5.1). For plotting, ChIP-seq signals were generated from processed bigwig files, mapped to genomic regions where H3K27ac peaks overlap with upregulated H3K27ac regions in HDI groups.

Chemical modifications of SAHA

Compound #1 (1 g, 10.74 mmol) was added to a solution of monomethyl adipate (2.02 g, 10.74 mmol), 1-Ethyl-3-(3-dimethylaminopropyl)carbodiimide (EDCI) (2.26 g, 11.81 mmol), and

4-Dimethylaminopyridine (DMAP) (1.57 g, 12.89 mmol) in 20 mL CH_2Cl_2 and stirred for 8 h at room temperature (RT). The mixture was successively washed with 1 M HCl, saturated NaHCO3 (30 mL), and saturated NaCl (30 mL), followed by organic phase separation, which was dried over anhydrous Na_2SO_4. After concentration, the resultant crude product was purified by silica gel column chromatography to get compound #2. NaOH (1.14 g, 28.48 mmol) was added to a solution of compound #2 (2.5 g, 9.49 mmol) in 20 mL MeOH/H_2O (5:1) and stirred at RT for 12 h. After solvent removal by rotary evaporation, the resulting residue was dissolved in 5 mL H_2O, the pH was adjusted to 1 with 1 M HCl, and the mixture was filtered. The filter cake was further purified by recrystallization with EtOH to get compound #3 (SAA). White solid, yield 97.2%. ^{1}H NMR (400 MHz, DMSO) δ 11.96 (s, 1H), 9.90 (s, 1H), 7.63-7.56 (m, 2H), 7.28 (t, $J = 7.9$ Hz, 2H), 7.06-6.97 (m, 1H), 2.29 (t, $J = 7.5$ Hz, 2H), 2.20 (t, $J = 7.3$ Hz, 2H), 1.63-1.44 (m, 4H), 1.37-1.24 (m, $J = 6.7$ Hz, 4H). ^{13}C NMR (101 MHz, DMSO) δ 175.02, 171.75, 139.81, 129.09, 123.38, 119.50, 36.82, 34.11, 28.87, 28.81, 25.47, 24.87. MS-ESI (*m/z*) calc. for $C_{37}H_{49}N_9O_6[2\,M + Na]^+$ 521.26, found 520.93.

DATA AVAILABILITY

RNA-seq data and ChIP-seq data are deposited in the Gene Expression Omnibus database. The AML12 cell RNA-seq accession number is GSE276094, and the reviewer token is avsbkckkpzilnmb. The AML12 ChIP-seq accession number is GSE276219, and the reviewer token is afmdwsecffcrhkb. The tumor RNA-seq accession number is GSE288240, and the reviewer token is enmjqewovbkxxsn.

ACKNOWLEDGEMENTS

We thank Drs. Xiang Zhang and Xu Zhan for guidance with the initial luciferase imaging, Drs. Bingning Dong and Wenliang Li for sharing plasmids, Drs. Wenshe Liu, Loning Fu, and Jeanine Van Nostrand for helpful discussions, and Fei Peng for assistance with mouse studies. We thank the Gene Vector Core at Baylor College of Medicine (BCM) for assistance with viral vector production, the Mouse Metabolism and Phenotyping Core at BCM (supported by NIH HG006348, DK114356, and HL130249) for luciferase imaging, and the Human Tissue Acquisition and Pathology Core at BCM (supported by CA125123) for histology studies. MJY was partially supported by the Institutional Research Grant at the University of Texas MD Anderson Cancer Center and the Leukemia & Lymphoma Society (LLS 6680-24). XH and HF were supported by the National Natural Science Foundation of China (22377068 and 22477070). PL and DG were supported by the Cancer Prevention and Research Institute of Texas (RR210029) and R37CA296577. UKS was supported by Frank Belton Kimmel and Sandra Kimmel Endowed Post-Doctoral Fellowship and training fellowship from the Gulf Coast Consortia (GCC) on the Training in Precision Environmental Health Sciences (TPEHS) Program (T32ES027801). The investigators were supported by ES034768, AG069966, and HL173243. The study was partially supported by the NIH grant R21CA215591.

AUTHOR CONTRIBUTIONS

C.R., X.L., and W.L. conducted animal studies. H.R. performed bioinformatics analyses of public databases, ChIP-seq, and RNA-seq. H.J. analyzed the CRISPR screen data. WL constructed recombinant DNA, conducted the CRISPR screen, and performed YF-related in vitro experiments. C.R. validated the dominant-negative effects of YF mutants and compiled RNA-seq results. X.L., Y.C., and H.F. conducted chemical modification of SAHA and characterization of SAA. C.C. assisted with cloning. M.J.Y. advised on the interpretation of histology data. P.L. and D.G. helped with ChIP-seq data analysis. U.K.S. and Y.S. helped with RNA-seq and figure plotting. Z.L. supervised the bioinformatics analysis of the CRISPR screen. L.H. supervised bioinformatics analysis of public databases. X.H. supervised the production and characterization of SAA. Z.S. conceived the study and supervised all other analyses. C.R., R.H., X.L., W.L., X.H., L.H., and Z.S. analyzed and interpreted the data. X.H. and Z.S. obtained the funding. C.R. and Z.S. wrote the manuscript with inputs from other authors. All the authors have read and approved the article.

ADDITIONAL INFORMATION

Supplementary information The online version contains supplementary material available at https://doi.org/10.1038/s41392-026-02698-1.

Conflict of interest: The authors declare no competing interests.

REFERENCES

1. Chen, H. P., Zhao, Y. T. & Zhao, T. C. Histone deacetylases and mechanisms of regulation of gene expression. *Crit. Rev. Oncog.* **20**, 35–47 (2015).
2. Seto, E. & Yoshida, M. Erasers of histone acetylation: the histone deacetylase enzymes. *Cold Spring Harb. Perspect. Biol.* **6**, a018713 (2014).
3. Porter, N. J. & Christianson, D. W. Structure, mechanism, and inhibition of the zinc-dependent histone deacetylases. *Curr. Opin. Struct. Biol.* **59**, 9–18 (2019).
4. Lahm, A. et al. Unraveling the hidden catalytic activity of vertebrate class IIa histone deacetylases. *Proc. Natl. Acad. Sci. U.S.A.* **104**, 17335–17340 (2007).
5. Fischle, W. et al. Enzymatic activity associated with class II HDACs is dependent on a multiprotein complex containing HDAC3 and SMRT/N-CoR. *Mol. Cell.* **9**, 45–57 (2002).
6. Khan, O. & La Thangue, N. B. HDAC inhibitors in cancer biology: emerging mechanisms and clinical applications. *Immunol. Cell Biol.* **90**, 85–94 (2012).
7. Ho, T. C. S., Chan, A. H. Y. & Ganesan, A. Thirty Years of HDAC Inhibitors: 2020 Insight and Hindsight. *J. Med Chem.* **63**, 12460–12484 (2020).
8. Robey, R. W. et al. Histone deacetylase inhibitors: emerging mechanisms of resistance. *Mol. Pharm.* **8**, 2021–2031 (2011).
9. Shi, M.-Q. et al. Advances in targeting histone deacetylase for treatment of solid tumors. *J. Hematol. Oncol.* **17**, 37 (2024).
10. Knipstein, J. & Gore, L. Entinostat for treatment of solid tumors and hematologic malignancies. *Expert Opin. Investig. Drugs.* **20**, 1455–1467 (2011).
11. Shah, R. R. Safety and Tolerability of Histone Deacetylase (HDAC) Inhibitors in Oncology. *Drug Saf.* **42**, 235–245 (2019).
12. Lauffer, B. E. et al. Histone deacetylase (HDAC) inhibitor kinetic rate constants correlate with cellular histone acetylation but not transcription and cell viability. *J. Biol. Chem.* **288**, 26926–43 (2013).
13. Lopez-Atalaya, J. P., Ito, S., Valor, L. M., Benito, E. & Barco, A. Genomic targets, and histone acetylation and gene expression profiling of neural HDAC inhibition. *Nucleic Acids Res.* **41**, 8072–8084 (2013).
14. Kasper, L. H. et al. CBP/p300 double null cells reveal effect of coactivator level and diversity on CREB transactivation. *EMBO J.* **29**, 3660–3672 (2010).
15. Halsall, J., Gupta, V., O'Neill, L. P., Turner, B. M. & Nightingale, K. P. Genes are often sheltered from the global histone hyperacetylation induced by HDAC inhibitors. *PLoS ONE.* **7**, e33453 (2012).
16. Sun, Z. et al. Deacetylase-independent function of HDAC3 in transcription and metabolism requires nuclear receptor corepressor. *Mol. Cell* **52**, 769–782 (2013).
17. Mullican, S. E. et al. Histone deacetylase 3 is an epigenomic brake in macrophage alternative activation. *Genes Dev.* **25**, 2480–2488 (2011).
18. Wilting, R. H. et al. Overlapping functions of Hdac1 and Hdac2 in cell cycle regulation and haematopoiesis. *EMBO J.* **29**, 2586–2597 (2010).
19. Parkin, G. Synthetic analogues relevant to the structure and function of zinc enzymes. *Chem. Rev.* **104**, 699–767 (2004).
20. Taylor, B. S. et al. Frequent alterations and epigenetic silencing of differentiation pathway genes in structurally rearranged liposarcomas. *Cancer Discov.* **1**, 587–597 (2011).
21. Ropero, S. et al. A truncating mutation of HDAC2 in human cancers confers resistance to histone deacetylase inhibition. *Nat. Genet.* **38**, 566–569 (2006).
22. Ropero, S. et al. Transforming pathways unleashed by a HDAC2 mutation in human cancer. *Oncogene.* **27**, 4008–4012 (2008).
23. Stark, M. & Hayward, N. Genome-wide loss of heterozygosity and copy number analysis in melanoma using high-density single-nucleotide polymorphism arrays. *Cancer Res.* **67**, 2632–2642 (2007).
24. Ree, A. H., Folkvord, S. & Flatmark, K. HDAC2 deficiency and histone acetylation. *Nat. Genet.* **40**, 812–813 (2008).
25. Hanigan, C. L. et al. An inactivating mutation in HDAC2 leads to dysregulation of apoptosis mediated by APAF1. *Gastroenterology.* **135**, 1654–1664.e2 (2008).
26. Hu, X.-T. et al. HDAC2 inhibits EMT-mediated cancer metastasis by down-regulating the long noncoding RNA H19 in colorectal cancer. *J. Exp. Clin. Cancer Res* **39**, 270 (2020).
27. Osada, H. et al. Reduced expression of class II histone deacetylase genes is associated with poor prognosis in lung cancer patients. *Int J. Cancer* **112**, 26–32 (2004).
28. Lv, Z. et al. Downregulation of HDAC6 promotes angiogenesis in hepatocellular carcinoma cells and predicts poor prognosis in liver transplantation patients. *Mol. Carcinog.* **55**, 1024–1033 (2016).
29. Zhang, Z. et al. HDAC6 expression is correlated with better survival in breast cancer. *Clin. Cancer Res* **10**, 6962–6968 (2004).
30. Lagger, S. et al. Crucial function of histone deacetylase 1 for differentiation of teratomas in mice and humans. *EMBO J.* **29**, 3992–4007 (2010).

31. Zrimšek, M. et al. HDAC1 acts as a tumor suppressor in ALK-positive anaplastic large cell lymphoma: implications for HDAC inhibitor therapy. *Leukemia* **39**, 1412–1424 (2025).
32. Santoro, F. et al. A dual role for Hdac1: oncosuppressor in tumorigenesis, oncogene in tumor maintenance. *Blood.* **121**, 3459–3468 (2013).
33. Bhaskara, S. et al. Hdac3 is essential for the maintenance of chromatin structure and genome stability. *Cancer Cell.* **18**, 436–447 (2010).
34. Song, C., Zhu, S., Wu, C. & Kang, J. Histone deacetylase (HDAC) 10 suppresses cervical cancer metastasis through inhibition of matrix metalloproteinase (MMP) 2 and 9 expression. *J. Biol. Chem.* **288**, 28021–28033 (2013).
35. Leslie, P. L. et al. Histone deacetylase 11 inhibition promotes breast cancer metastasis from lymph nodes. *Nat. Commun.* **10**, 4192 (2019).
36. Jung, K. H. et al. Histone deacetylase 6 functions as a tumor suppressor by activating c-Jun NH2-terminal kinase-mediated beclin 1-dependent autophagic cell death in liver cancer. *Hepatology* **56**, 644–657 (2012).
37. Xie, J., Liu, R., Cai, Y. & Liu, D. HDAC1: a promising target for cancer treatment: insights from a thorough analysis of tumor functions. *Transl. Cancer Res* **13**, 5300–5315 (2024).
38. Li, R., Wu, X., Zhao, P., Xue, K. & Li, J. A pan-cancer analysis identifies HDAC11 as an immunological and prognostic biomarker. *FASEB J.* **36**, e22326 (2022).
39. Chen, H. et al. A pancancer analysis of histone deacetylase 3 in human tumors. *Transl. Cancer Res* **13**, 65–80 (2024).
40. Zhou, Z. et al. HDAC11 mediates the ubiquitin-dependent degradation of p53 and inhibits the anti-leukemia effect of PD0166285. *Med Oncol.* **40**, 325 (2023).
41. ICGC/TCGA Pan-Cancer Analysis of Whole Genomes Consortium. Pan-cancer analysis of whole genomes. *Nature* **578**, 82–93 (2020).
42. Miao, D. et al. Genomic correlates of response to immune checkpoint therapies in clear cell renal cell carcinoma. *Science* **359**, 801–806 (2018).
43. Sammut, S.-J. et al. Multi-omic machine learning predictor of breast cancer therapy response. *Nature.* **601**, 623–629 (2022).
44. Kinnersley, B. et al. Analysis of 10,478 cancer genomes identifies candidate driver genes and opportunities for precision oncology. *Nat. Genet* **56**, 1868–1877 (2024).
45. Jee, J. et al. Automated real-world data integration improves cancer outcome prediction. *Nature.* **636**, 728–736 (2024).
46. Sinha, S. et al. PERCEPTION predicts patient response and resistance to treatment using single-cell transcriptomics of their tumors. *Nat. Cancer* **5**, 938–952 (2024).
47. Zucker, M. et al. Pan-cancer analysis of biallelic inactivation in tumor suppressor genes identifies KEAP1 zygosity as a predictive biomarker in lung cancer. *Cell* **188**, 851–867.e17 (2025).
48. Zhang, J. et al. Pan-cancer analysis of the transcriptional expression of histone acetylation enzymes in solid tumors defines a new classification scheme for gliomas. *Front Immunol.* **15**, 1523034 (2024).
49. Mansoori, B., Mohammadi, A., Davudian, S., Shirjang, S. & Baradaran, B. The Different Mechanisms of Cancer Drug Resistance: A Brief Review. *Adv. Pharm. Bull.* **7**, 339–348 (2017).
50. Joung, J. et al. Genome-scale CRISPR-Cas9 knockout and transcriptional activation screening. *Nat. Protoc.* **12**, 828–863 (2017).
51. Jeong, H.-H., Kim, S. Y., Rousseaux, M. W. C., Zoghbi, H. Y. & Liu, Z. Beta-binomial modeling of CRISPR pooled screen data identifies target genes with greater sensitivity and fewer false negatives. *Genome Res* **29**, 999–1008 (2019).
52. Ma, J. et al. Trichostatin A, a histone deacetylase inhibitor, suppresses proliferation and promotes apoptosis of esophageal squamous cell lines. *Mol. Med Rep.* **11**, 4525–4531 (2015).
53. Duan, H., Heckman, C. A. & Boxer, L. M. Histone deacetylase inhibitors down-regulate bcl-2 expression and induce apoptosis in t(14;18) lymphomas. *Mol. Cell Biol.* **25**, 1608–1619 (2005).
54. Bolden, J. E. et al. HDAC inhibitors induce tumor-cell-selective pro-apoptotic transcriptional responses. *Cell Death Dis.* **4**, e519 (2013).
55. He, L. et al. Mcl-1 and FBW7 control a dominant survival pathway underlying HDAC and Bcl-2 inhibitor synergy in squamous cell carcinoma. *Cancer Discov.* **3**, 324–337 (2013).
56. Kunami, N., Katsuya, H., Nogami, R., Ishitsuka, K. & Tamura, K. Promise of combining a Bcl-2 family inhibitor with bortezomib or SAHA for adult T-cell leukemia/lymphoma. *Anticancer Res* **34**, 5287–5294 (2014).
57. Cyrenne, B. M. et al. Synergy of BCL2 and histone deacetylase inhibition against leukemic cells from cutaneous T-cell lymphoma patients. *Blood* **130**, 2073–2083 (2017).
58. Martin, A. P. et al. BCL-2 family inhibitors enhance histone deacetylase inhibitor and sorafenib lethality via autophagy and overcome blockade of the extrinsic pathway to facilitate killing. *Mol. Pharm.* **76**, 327–341 (2009).
59. Berghauser Pont, L. M. E. et al. The Bcl-2 inhibitor Obatoclax overcomes resistance to histone deacetylase inhibitors SAHA and LBH589 as radiosensitizers in patient-derived glioblastoma stem-like cells. *Genes Cancer* **5**, 445–459 (2014).
60. Citro, S. et al. Synergistic antitumour activity of HDAC inhibitor SAHA and EGFR inhibitor gefitinib in head and neck cancer: a key role for ΔNp63α. *Br. J. Cancer* **120**, 658–667 (2019).
61. Ouaïssi, M. et al. Histone deacetylase (HDAC) encoding gene expression in pancreatic cancer cell lines and cell sensitivity to HDAC inhibitors. *Cancer Biol. Ther.* **7**, 523–531 (2008).
62. Moreaux, J. et al. Gene expression-based prediction of myeloma cell sensitivity to histone deacetylase inhibitors. *Br. J. Cancer* **109**, 676–685 (2013).
63. Geeleher, P. et al. Predicting Response to Histone Deacetylase Inhibitors Using High-Throughput Genomics. *J. Natl. Cancer Inst.* **107**, djv247 (2015).
64. Mayr, C. et al. HDAC Screening Identifies the HDAC Class I Inhibitor Romidepsin as a Promising Epigenetic Drug for Biliary Tract Cancer. *Cancers (Basel)* **13**, 3862 (2021).
65. Behnisch-Cornwell, S. et al. Correlation Analysis of Protein Expression of 10 HDAC/Sirtuin Isoenzymes with Sensitivities of 23 Anticancer Drugs in 17 Cancer Cell Lines and Potentiation of Drug Activity by Co-Treatment with HDAC Inhibitors. *Cancers (Basel)* **14**, 187 (2021).
66. Fotheringham, S. et al. Genome-wide loss-of-function screen reveals an important role for the proteasome in HDAC inhibitor-induced apoptosis. *Cancer Cell* **15**, 57–66 (2009).
67. Kim, D., Kim, S. H., Yoon, C. & Lee, G. M. Genome-wide CRISPR/Cas9 knockout screening to mitigate cell growth inhibition induced by histone deacetylase inhibitors in recombinant CHO cells. *Biotechnol. Bioeng.* **121**, 931–941 (2024).
68. Cai, Y. et al. The effects of a histone deacetylase inhibitor on biological behavior of diffuse large B-cell lymphoma cell lines and insights into the underlying mechanisms. *Cancer Cell Int.* **13**, 57 (2013).
69. Yang, H. et al. Pharmaco-transcriptomic correlation analysis reveals novel responsive signatures to HDAC inhibitors and identifies Dasatinib as a synergistic interactor in small-cell lung cancer. *EBioMedicine* **69**, 103457 (2021).
70. Hagelkruys, A. et al. Essential Nonredundant Function of the Catalytic Activity of Histone Deacetylase 2 in Mouse Development. *Mol. Cell Biol.* **36**, 462–474 (2016).
71. Kwapis, J. L. et al. Context and Auditory Fear are Differentially Regulated by HDAC3 Activity in the Lateral and Basal Subnuclei of the Amygdala. *Neuropsychopharmacology.* **42**, 1284–1294 (2017).
72. Humphrey, G. W. et al. Complementary roles for histone deacetylases 1, 2, and 3 in differentiation of pluripotent stem cells. *Differentiation* **76**, 348–356 (2008).
73. Sekhavat, A., Sun, J.-M. & Davie, J. R. Competitive inhibition of histone deacetylase activity by trichostatin A and butyrate. *Biochem Cell Biol.* **85**, 751–758 (2007).
74. Senese, S. et al. Role for histone deacetylase 1 in human tumor cell proliferation. *Mol. Cell Biol.* **27**, 4784–4795 (2007).
75. Oger, F. et al. Pharmacological HDAC inhibition impairs pancreatic β-cell function through an epigenome-wide reprogramming. *iScience* **26**, 107231 (2023).
76. Armour, S. M. et al. An HDAC3-PROX1 corepressor module acts on HNF4α to control hepatic triglycerides. *Nat. Commun.* **8**, 549 (2017).
77. Gao, T. & Qian, J. EnhancerAtlas 2.0: an updated resource with enhancer annotation in 586 tissue/cell types across nine species. *Nucleic Acids Res* **48**, D58–D64 (2020).
78. Chen, X. & Calvisi, D. F. Hydrodynamic transfection for generation of novel mouse models for liver cancer research. *Am. J. Pathol.* **184**, 912–923 (2014).
79. Russell, J. O. & Monga, S. P. Wnt/β-Catenin Signaling in Liver Development, Homeostasis, and Pathobiology. *Annu Rev. Pathol.* **13**, 351–378 (2018).
80. Bouattour, M. et al. Recent developments of c-Met as a therapeutic target in hepatocellular carcinoma. *Hepatology* **67**, 1132–1149 (2018).
81. Lin, C.-P., Liu, C.-R., Lee, C.-N., Chan, T.-S. & Liu, H. E. Targeting c-Myc as a novel approach for hepatocellular carcinoma. *World J. Hepatol.* **2**, 16–20 (2010).
82. Tao, J. et al. Modeling a human hepatocellular carcinoma subset in mice through coexpression of met and point-mutant β-catenin. *Hepatology* **64**, 1587–1605 (2016).
83. Vaidya, A. S. et al. Novel histone deacetylase 8 ligands without a zinc chelating group: exploring an 'upside-down' binding pose. *Bioorg. Med Chem. Lett.* **22**, 6621–6627 (2012).
84. Bieliauskas, A. V., Weerasinghe, S. V. W. & Pflum, M. K. H. Structural requirements of HDAC inhibitors: SAHA analogs functionalized adjacent to the hydroxamic acid. *Bioorg. Med Chem. Lett.* **17**, 2216–2219 (2007).
85. Bieliauskas, A. V., Weerasinghe, S. V. W., Negmeldin, A. T. & Pflum, M. K. H. Structural Requirements of Histone Deacetylase Inhibitors: SAHA Analogs Modified on the Hydroxamic Acid. *Arch. Pharm. (Weinh.)* **349**, 373–382 (2016).
86. Shields, N. J. et al. Late-stage MC38 tumours recapitulate features of human colorectal cancer - implications for appropriate timepoint selection in preclinical studies. *Front Immunol.* **14**, 1152035 (2023).
87. Chang, Y. et al. Development of a First-in-Class DNMT1/HDAC Inhibitor with Improved Therapeutic Potential and Potentiated Antitumor Immunity. *J. Med Chem.* **67**, 16480–16504 (2024).
88. Kodumudi, K. N. et al. Immune Checkpoint Blockade to Improve Tumor Infiltrating Lymphocytes for Adoptive Cell Therapy. *PLoS One* **11**, e0153053 (2016).

89. Wang, D. et al. Targeting EZH2 Reprograms Intratumoral Regulatory T Cells to Enhance Cancer Immunity. *Cell Rep.* **23**, 3262–3274 (2018).
90. Song, C.-H. et al. Combination treatment with 17β-estradiol and anti-PD-L1 suppresses MC38 tumor growth by reducing PD-L1 expression and enhancing M1 macrophage population in MC38 colon tumor model. *Cancer Lett.* **543**, 215780 (2022).
91. LaBonte, M. J. et al. DNA microarray profiling of genes differentially regulated by the histone deacetylase inhibitors vorinostat and LBH589 in colon cancer cell lines. *BMC Med Genomics* **2**, 67 (2009).
92. Roy, S., Jeffrey, R. & Tenniswood, M. Array-based analysis of the effects of trichostatin A and CG-1521 on cell cycle and cell death in LNCaP prostate cancer cells. *Mol. Cancer Ther.* **7**, 1931–1939 (2008).
93. Johnstone, R. W. & Licht, J. D. Histone deacetylase inhibitors in cancer therapy: is transcription the primary target? *Cancer Cell* **4**, 13–18 (2003).
94. Wardell, S. E. et al. Glucose metabolism as a target of histone deacetylase inhibitors. *Mol. Endocrinol.* **23**, 388–401 (2009).
95. Gupta, P., Ho, P.-C., Ha, S. G., Lin, Y.-W. & Wei, L.-N. HDAC3 as a molecular chaperone for shuttling phosphorylated TR2 to PML: a novel deacetylase activity-independent function of HDAC3. *PLoS ONE* **4**, e4363 (2009).
96. Yin, H. et al. HDAC3 controls male fertility through enzyme-independent transcriptional regulation at the meiotic exit of spermatogenesis. *Nucleic Acids Res* **49**, 5106–5123 (2021).
97. You, S.-H. et al. Nuclear receptor co-repressors are required for the histone-deacetylase activity of HDAC3 in vivo. *Nat. Struct. Mol. Biol.* **20**, 182–187 (2013).
98. Poleshko, A. et al. Genome-Nuclear Lamina Interactions Regulate Cardiac Stem Cell Lineage Restriction. *Cell* **171**, 573–587.e14 (2017).
99. Lewandowski, S. L., Janardhan, H. P. & Trivedi, C. M. Histone Deacetylase 3 Coordinates Deacetylase-independent Epigenetic Silencing of Transforming Growth Factor-β1 (TGF-β1) to Orchestrate Second Heart Field Development. *J. Biol. Chem.* **290**, 27067–27089 (2015).
100. Ren, J. et al. Deacetylase-dependent and -independent role of HDAC3 in cardiomyopathy. *J. Cell Physiol.* **238**, 647–658 (2023).
101. Qian, S. et al. Enzyme-independent functions of HDAC3 in the adult heart. *Acta Pharm. Sin. B* **15**, 3561–3574 (2025).
102. Jung, H. et al. Deacetylase activity-independent transcriptional activation by HDAC2 during TPA-induced HL-60 cell differentiation. *PLoS One* **13**, e0202935 (2018).
103. Jensen, E. D., Schroeder, T. M., Bailey, J., Gopalakrishnan, R. & Westendorf, J. J. Histone deacetylase 7 associates with Runx2 and represses its activity during osteoblast maturation in a deacetylation-independent manner. *J. Bone Min. Res* **23**, 361–372 (2008).
104. Brinkmann, H. et al. Histone hyperacetylation induced by histone deacetylase inhibitors is not sufficient to cause growth inhibition in human dermal fibroblasts. *J. Biol. Chem.* **276**, 22491–22499 (2001).
105. Halasa, M. et al. Deacetylation of Transcription Factors in Carcinogenesis. *Int J. Mol. Sci.* **22**, 11810 (2021).
106. Cao, L.-L. et al. Histone deacetylase HDAC1 expression correlates with the progression and prognosis of lung cancer: A meta-analysis. *Med. (Baltim.)* **96**, e7663 (2017).
107. Bi, L. et al. HDAC11 Regulates Glycolysis through the LKB1/AMPK Signaling Pathway to Maintain Hepatocellular Carcinoma Stemness. *Cancer Res* **81**, 2015–2028 (2021).
108. Oltra, S. S. et al. HDAC5 Inhibitors as a Potential Treatment in Breast Cancer Affecting Very Young Women. *Cancers (Basel)* **12**, 412 (2020).
109. Li, W. & Sun, Z. Mechanism of Action for HDAC Inhibitors-Insights from Omics Approaches. *Int. J. Mol. Sci.* **20**, 1616 (2019).
110. Gu, X. et al. SAMTOR is an S-adenosylmethionine sensor for the mTORC1 pathway. *Science* **358**, 813–818 (2017).
111. Tward, A. D. et al. Distinct pathways of genomic progression to benign and malignant tumors of the liver. *Proc. Natl. Acad. Sci. USA* **104**, 14771–14776 (2007).
112. Mátés, L. et al. Molecular evolution of a novel hyperactive Sleeping Beauty transposase enables robust stable gene transfer in vertebrates. *Nat. Genet* **41**, 753–761 (2009).
113. Ruiz de Galarreta, M. et al. β-Catenin Activation Promotes Immune Escape and Resistance to Anti-PD-1 Therapy in Hepatocellular Carcinoma. *Cancer Discov.* **9**, 1124–1141 (2019).
114. ENCODE Project Consortium. An integrated encyclopedia of DNA elements in the human genome. *Nature.* **489**, 57–74 (2012).